Electromagnetic Scattering by Nonspherical Particles

Michael I. Mishchenko and Larry D. Travis

NASA Goddard Institute for Space Studies,
2880 Broadway, New York, New York 10025, U.S.A.

Abstract. The knowledge of absorption and scattering characteristics of small particles is required for a reliable evaluation of the climate forcing caused by clouds and aerosols as well as for studying the physical and chemical properties of atmospheric particulates using remote sensing techniques. Since many particles suspended in the atmosphere are nonspherical, their optical properties may not be adequately described by the classical Lorenz-Mie theory and must be determined using advanced theoretical and experimental techniques. In this chapter, we describe how electromagnetic scattering by small nonspherical particles can be computed and measured; analyze the main effects of nonsphericity on electromagnetic scattering; and discuss various implications of these effects in computations of the earth's radiation balance and atmospheric remote sensing.

1 Introduction

Aerosols and clouds affect the earth's radiation balance by scattering and absorbing the short-wave radiation coming from the sun and the long-wave radiation emitted by the surface. The evaluation of this radiative effect requires the knowledge of the optical properties of aerosol and cloud particles (Lacis and Mishchenko 1995; Rossow and Schiffer 1999). This knowledge is also needed for analyses of remote sensing measurements based on passive and active techniques (Stephens 1994).

Although it is well recognized that many particles suspended in the atmosphere are nonspherical, the convenient availability of the Lorenz-Mie theory has led to the widespread practice of treating their optical properties as if the particles were perfect spheres. However, it is becoming increasingly obvious that this approach can cause significant quantitative errors and must be replaced by an analysis strategy based on specific knowledge of scattering and absorption characteristics of nonspherical particles. This improved strategy has been made possible by recent advances in numerical and experimental techniques and the rapid improvement of scientific workstations (Mishchenko et al. 2000a).

In this chapter we first introduce the necessary theoretical concepts and terminology and describe how the optical properties of nonspherical particles can be computed theoretically and measured using modern laboratory techniques. Then we discuss the main effects of nonsphericity on electromagnetic

In *Expolring the Atmosphere by Remote Sensing Techniques*
R. Guzzi, Editor (Springer-Verlag, Berlin, 2003), pp. 77−127

scattering patterns and stress the need for a statistical approach in modeling scattering and absorption characteristics of size and shape distributions of natural aerosol and cloud particles. Finally, we demonstrate how particle nonsphericity can affect computations of the earth's radiation balance and analyses of remote sensing measurements.

2 Polarization Characteristics of Electromagnetic Radiation

The mathematical description of all classical optics phenomena is based on the Maxwell equations for the macroscopic electromagnetic field (Jackson 1998):

$$\nabla \cdot \mathbf{D} = \rho, \tag{1}$$

$$\nabla \times \mathbf{E} = -\partial \mathbf{B}/\partial t, \tag{2}$$

$$\nabla \cdot \mathbf{B} = 0, \tag{3}$$

$$\nabla \times \mathbf{H} = \mathbf{J} + \partial \mathbf{D}/\partial t, \tag{4}$$

where t is time, $\mathbf{E}$ the electric and $\mathbf{H}$ the magnetic field, $\mathbf{B}$ the magnetic induction, $\mathbf{D}$ the electric displacement, and ρ and $\mathbf{J}$ the macroscopic charge density and current density, respectively. All quantities appearing in the Maxwell equations are functions of time and spatial coordinates. The vector fields entering (1)–(4) are related by

$$\mathbf{D} = \varepsilon_0 \mathbf{E} + \mathbf{P}, \tag{5}$$

$$\mathbf{H} = \mathbf{B}/\mu_0 - \mathbf{M}, \tag{6}$$

where $\mathbf{P}$ is the electric polarization, $\mathbf{M}$ the magnetization, and ε_0 the electric permittivity and μ_0 the magnetic permeability of free space. Equations (1)–(6) are insufficient for a unique determination of the electric and magnetic fields from a given distribution of charges and currents and must be supplemented with the constitutive relations

$$\mathbf{J} = \sigma \mathbf{E}, \tag{7}$$

$$\mathbf{B} = \mu \mathbf{H}, \tag{8}$$

$$\mathbf{P} = \varepsilon_0 \chi \mathbf{E}\,, \tag{9}$$

where σ is the conductivity, μ the permeability, and χ the electric susceptibility. For linear and isotropic media, σ, μ, and χ are scalars independent of the fields.

The field vectors $\mathbf{E}$, $\mathbf{D}$, $\mathbf{B}$, and $\mathbf{H}$ may be discontinuous across an interface separating one medium from another. The boundary conditions at such an interface can be derived from the integral equivalents of the Maxwell equations:

$$\begin{array}{l}(\mathbf{D}_2-\mathbf{D}_1)\cdot\hat{n}=\rho_S,\ \ \hat{n}\times(\mathbf{H}_2-\mathbf{H}_1)=0 \quad \text{(finite conductivity)}\\ (\mathbf{B}_2-\mathbf{B}_1)\cdot\hat{n}=0,\quad \hat{n}\times(\mathbf{E}_2-\mathbf{E}_1)=0\ ,\end{array} \tag{10}$$

where $\hat{n}$ is the local normal to the interface separating media 1 and 2 and pointing toward medium 2 and ρ_S is the surface charge density. The boundary conditions (10) are useful in solving the Maxwell equations in different adjacent regions with continuous physical properties and then linking the partial solutions to determine the fields throughout all space.

A fundamental feature of the Maxwell equations is that they allow for a simple traveling wave solution which represents the transport of electromagnetic energy from one point to another and embodies the concept of a perfectly monochromatic parallel beam of light. This solution is a plane electromagnetic wave propagating in a homogeneous medium without sources and is given by

$$\mathbf{E}(\mathbf{r},t)=\mathbf{E}_0\ \exp(\mathrm{i}\mathbf{k}\cdot\mathbf{r}-\mathrm{i}\omega t),\quad \mathbf{H}(\mathbf{r},t)=\mathbf{H}_0\ \exp(\mathrm{i}\mathbf{k}\cdot\mathbf{r}-\mathrm{i}\omega t). \tag{11}$$

The vectors $\mathbf{E}_0, \mathbf{H}_0$, and $\mathbf{k}$ are assumed to be constant and the wave vector $\mathbf{k}$ may, in general, be complex: $\mathbf{k}=\mathbf{k}_\mathrm{R}+\mathrm{i}\mathbf{k}_\mathrm{I}$. Hence,

$$\mathbf{E}(\mathbf{r},t)=\mathbf{E}_0\ \exp(-\mathbf{k}_1\cdot\mathbf{r})\ \exp(\mathrm{i}\mathbf{k}_\mathrm{R}\cdot\mathbf{r}-\mathrm{i}\omega t), \tag{12}$$

$$\mathbf{H}(\mathbf{r},t)=\mathbf{H}_0\ \exp(-\mathbf{k}_1\cdot\mathbf{r})\ \exp(\mathrm{i}\mathbf{k}_\mathrm{R}\cdot\mathbf{r}-\mathrm{i}\omega t). \tag{13}$$

$\mathbf{E}_0\ \exp(-\mathbf{k}_\mathrm{I}\cdot\mathbf{r})$ and $\mathbf{H}_0\ \exp(-\mathbf{k}_\mathrm{I}\cdot\mathbf{r})$ are the amplitudes of the electric and magnetic waves, while $\mathbf{k}_\mathrm{R}\cdot\mathbf{r}-\omega t$ is their phase. $\mathbf{k}_\mathrm{R}$ is normal to the surfaces of constant phase, whereas $\mathbf{k}_\mathrm{I}$ is normal to the surfaces of constant amplitude. The electromagnetic wave is called homogeneous when $\mathbf{k}_\mathrm{R}$ and $\mathbf{k}_\mathrm{I}$ are parallel; otherwise it is called inhomogeneous. Surfaces of constant phase propagate in the direction of $\mathbf{k}_\mathrm{R}$ with the phase velocity $\nu=\omega/|\mathbf{k}_\mathrm{R}|$.

The Maxwell equations for the plane wave take the form

$$\mathbf{k}\cdot\mathbf{E}_0=0, \tag{14}$$

$$\mathbf{k}\cdot\mathbf{H}_0=0, \tag{15}$$

$$\mathbf{k}\times\mathbf{E}_0=\omega\mu\mathbf{H}_0, \tag{16}$$

$$\mathbf{k}\times\mathbf{H}_0=-\omega\varepsilon\mathbf{E}_0, \tag{17}$$

where $\varepsilon=\varepsilon_0(1+\chi)+\mathrm{i}\sigma/\omega$ is the complex permittivity. The first two equations indicate that the plane electromagnetic wave is transverse: both $\mathbf{E}_0$ and $\mathbf{H}_0$ are perpendicular to $\mathbf{k}$. Furthermore, $\mathbf{E}_0$ and $\mathbf{H}_0$ are mutually perpendicular. Equations (11) and (16) yield $\mathbf{H}(\mathbf{r},t)=(\omega\mu)^{-1}\mathbf{k}\times\mathbf{E}(\mathbf{r},t)$. Therefore, a plane electromagnetic wave can always be considered in terms of only the electric field.

By taking the vector product of both sides of (16) with $\mathbf{k}$ and using (14) and (17), we have $\mathbf{k}\cdot\mathbf{k}=\omega^2\varepsilon\mu$ In the practically important case of a homogeneous plane wave, the complex wave vector can be written as $\mathbf{k}=$

$(\mathrm{k_R} + \mathrm{ik_I})\hat{n}$ where $\hat{n}$ is a real unit vector in the direction of propagation and both $\mathrm{k_R}$ and $\mathrm{k_I}$ are nonnegative. We then obtain

$$\mathrm{k} = \mathrm{k_R} + \mathrm{ik_I} = \omega\sqrt{\varepsilon\mu} = \omega\mathrm{m}/c, \tag{18}$$

where k is the wave number, $c = 1\,\big/\sqrt{\varepsilon_0\mu_0}$ is the speed of light in a vacuum, and

$$\mathrm{m} = \mathrm{m_R} + \mathrm{im_I} = \sqrt{\varepsilon\mu/\varepsilon_0\mu_0} = c\sqrt{\varepsilon\mu} \tag{19}$$

is the complex refractive index with nonnegative real, $\mathrm{m_R}$, and imaginary, $\mathrm{m_I}$, parts. Thus, the plane homogeneous wave has the form

$$\mathbf{E}(\mathbf{r},t) = \mathbf{E}(\mathbf{r})e^{-\mathrm{i}\omega t} = \mathbf{E}_0\,\exp\left(-\omega c^{-1}\mathrm{m_I}\hat{n}\cdot\mathbf{r}\right)\,\exp\left(-\mathrm{i}\omega c^{-1}\mathrm{m_R}\hat{n}\cdot\mathbf{r} - \mathrm{i}\omega t\right). \tag{20}$$

If the imaginary part of the refractive index is nonzero, then it determines the decay of the amplitude of the wave as it propagates through the medium. In this case the medium is absorbing. The real part of the refractive index determines the phase velocity of the wave: $\nu = c/\mathrm{m_R}$. For a vacuum, $\mathrm{m} = \mathrm{m_R} = 1$ and $\nu = c$. The time-averaged Poynting vector of the homogeneous plane wave is

$$\langle\mathbf{S}(\mathbf{r})\rangle = \frac{1}{2}\,\mathrm{Re}\,[\mathbf{E}(\mathbf{r})\times\mathbf{H}^*(\mathbf{r})] = \frac{1}{2}\,\mathrm{Re}\,\left\{\sqrt{\varepsilon/\mu}\right\}|\mathbf{E}_0|^2\,\exp(-2\omega c^{-1}\mathrm{m_I}\hat{n}\cdot\mathbf{r})\hat{n}. \tag{21}$$

Thus, $\langle\mathbf{S}(\mathbf{r})\rangle$ is in the direction of propagation and its absolute value $I(\mathbf{r}) = |\langle\mathbf{S}(\mathbf{r})\rangle|$, called intensity, is exponentially attenuated if the medium is absorbing: $I(\mathbf{r}) = I(0)\,\exp(-\alpha\hat{n}\cdot\mathbf{r})$. The absorption coefficient is $\alpha = 4\pi\mathrm{m_I}/\lambda$, where $\lambda = 2\pi c/\omega$ is the free-space wavelength. The intensity has the dimension of monochromatic energy flux: [energy/(area × time)].

Most photometric and polarimetric optical instruments cannot measure the fields associated with a beam of light but rather measure quantities that are time averages of quadratic combinations of field vector components and have the dimension of the intensity. To define these quantities, we will use the spherical coordinate system associated with a fixed right-handed Cartesian coordinate system (Fig. 1). The direction of propagation of a plane electromagnetic wave is specified by a unit vector $\hat{n}$ or, equivalently, by a couple (ϑ,φ), where $\vartheta\in[0,\pi]$ is the polar angle and $\varphi\in[0,2\pi]$ is the azimuth angle. The ϑ and φ components of the electric field vector are denoted as $\mathbf{E}_\vartheta$ and $\mathbf{E}_\varphi$, respectively. The component $\mathbf{E}_\vartheta = E_\vartheta\hat{\vartheta}$ lies in the meridional plane, whereas the component $\mathbf{E}_\varphi = E_\varphi\hat{\varphi}$ is perpendicular to this plane; $\hat{\vartheta}$ and $\hat{\varphi}$ are the corresponding unit vectors such that $\hat{n} = \hat{\vartheta}\times\hat{\varphi}$. Consider a plane electromagnetic wave propagating in a homogeneous nonabsorbing medium ($\mathrm{k_I} = 0$) and given by

$$\mathbf{E}(\mathbf{r},t) = \mathbf{E}_0\,\exp(\mathrm{ik}\hat{n}\cdot\mathbf{r} - \mathrm{i}\omega t). \tag{22}$$

The so-called Stokes parameters I, Q, U, and V are then defined as the elements of a real 4×1 column vector $\mathbf{I}$, otherwise known as the Stokes vector, as follows:

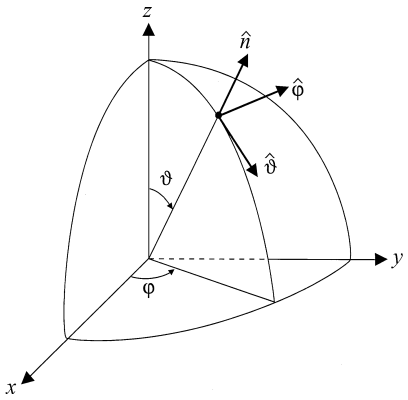

Fig. 1. Spherical coordinate system used to define the Stokes parameters.

$$\mathsf{I} = \begin{bmatrix} I \\ Q \\ U \\ V \end{bmatrix} = \frac{1}{2}\sqrt{\frac{\varepsilon}{\mu}} \begin{bmatrix} E_{0\vartheta}E_{0\vartheta}^* + E_{0\varphi}E_{0\varphi}^* \\ E_{0\vartheta}E_{0\vartheta}^* - E_{0\varphi}E_{0\varphi}^* \\ -E_{0\vartheta}E_{0\varphi}^* - E_{0\varphi}E_{0\vartheta}^* \\ \mathrm{i}(E_{0\varphi}E_{0\vartheta}^* - E_{0\vartheta}E_{0\varphi}^* \end{bmatrix}. \tag{23}$$

The first Stokes parameter, I, is equal to the intensity [(21) with with $\mathrm{m_I} = 0$ and real ε and μ]. The Stokes parameters Q, U, and V have the same dimension of monochromatic energy flux and describe the polarization state of the wave. It is easy to verify that the Stokes parameters are related by the identity

$$I^2 \equiv Q^2 + U^2 + V^2. \tag{24}$$

The definition of a monochromatic plane electromagnetic wave given by (22) implies that the complex amplitude $\mathbf{E}_0$ is constant. In reality, this quantity often fluctuates in time. Although the typical frequency of fluctuations is much smaller than the angular frequency ω, it is still so high that most optical devices are incapable of tracing the instantaneous values of the Stokes parameters but rather measure averages of Stokes parameters over a relatively long period of time. Therefore, we must modify the definition of the Stokes parameters for such *quasi-monochromatic* beam of light as follows:

$$\begin{bmatrix} I \\ Q \\ U \\ V \end{bmatrix} = \frac{1}{2}\sqrt{\frac{\varepsilon}{\mu}} \begin{bmatrix} \langle E_{0\vartheta}E_{0\vartheta}^* \rangle + \langle E_{0\varphi}E_{0\varphi}^* \rangle \\ \langle E_{0\vartheta}E_{0\vartheta}^* \rangle - \langle E_{0\varphi}E_{0\varphi}^* \rangle \\ -\langle E_{0\vartheta}E_{0\varphi}^* \rangle - \langle E_{0\varphi}E_{0\vartheta}^* \rangle \\ \mathrm{i}\langle E_{0\varphi}E_{0\vartheta}^* \rangle - \mathrm{i}\langle E_{0\vartheta}E_{0\varphi}^* \rangle \end{bmatrix}, \tag{25}$$

where $\langle ... \rangle$ denotes an average over a time interval long compared with the typical period of fluctuation. When two or more quasi-monochromatic beams

propagating in the same direction are mixed incoherently (i.e., assuming no permanent phase relationships between the separate beams), the Stokes vector of the mixture is equal to the sum of the Stokes vectors of the individual beams:

$$\mathbf{I} = \sum_n \mathbf{I}_n, \tag{26}$$

where n numbers the beams.

The identity (24) is not, in general, valid for a quasi-monochromatic beam. Instead, we have (Chandrasekhar 1960; Mishchenko et al. 2001)

$$I^2 \geq Q^2 + U^2 + V^2. \tag{27}$$

The equality holds only if $E_{0\vartheta}(t)$ and $E_{0\varphi}(t)$ are completely correlated. In this case the beam is said to be fully (or completely) polarized. This definition includes a monochromatic wave, but is more general. If $E_{0\vartheta}(t)$ and $E_{0\varphi}(t)$ are totally uncorrelated and $\langle E_{0\vartheta} E_{0\vartheta}^* \rangle = \langle E_{0\varphi} E_{0\varphi}^* \rangle$, then $Q = U = V = 0$, and the quasi-monochromatic beam of light is said to be unpolarized (or natural). In view of (27), it is always possible to *mathematically* decompose any quasi-monochromatic beam into two parts, one unpolarized with a Stokes vector $[I - \sqrt{Q^2 + U^2 + V^2}, 0, 0, 0]^\top$, and one fully polarized, with a Stokes vector $[\sqrt{Q^2 + U^2 + V^2}, Q, U, V]^\top$, where $\top$ stands for "transpose." Thus the intensity of the fully polarized component is $\sqrt{Q^2 + U^2 + V^2}$ so that the degree of (elliptical) polarization of the quasi-monochromatic beam is $P = \sqrt{Q^2 + U^2 + V^2}/I$. P vanishes for unpolarized light and is equal to 1 for fully polarized light. For a partially polarized beam ($0 < P < 1$) with $V \neq 0$, the sign of V indicates the preferential handedness of the vibration ellipses described by the endpoint of the electric vector: a positive V indicates left-handed polarization (the endpoint of the electric vector preferentially rotates in the anti-clockwise direction when viewed by an observer looking in the direction of light propagation) and a negative V indicates right-handed polarization. When $U = 0$, the ratio $P_Q = -Q/I$ is often called the degree of linear polarization. P_Q is positive when the vibrations of the electric vector in the φ direction (i.e., in the direction perpendicular to the meridional plane of the beam) dominate those in the ϑ direction, and is negative otherwise.

3 Scattering, Absorption, and Emission by an Arbitrary Particle

The presence of an object with an index of refraction different from that of the surrounding medium changes the electromagnetic field that would otherwise exist in an unbounded homogeneous space. The difference of the total field in the presence of the object and the original field that would exist in the absence of the object can be thought of as the field *scattered* by the object.

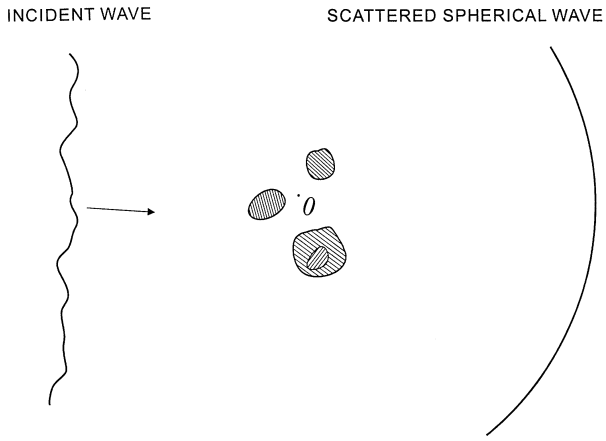

Fig. 2. Schematic representation of the electromagnetic scattering problem.

Hence, the total field is equal to the vector sum of the *incident* (original) field and the *scattered* field.

Consider a finite scattering object in the form of a single body or an aggregate imbedded in an infinite, homogeneous, nonabsorbing medium (Fig. 2). Mathematically this is equivalent to dividing all space into two regions: the finite interior region $V_{\rm INT}$ occupied by the scatterer and the infinite exterior region $V_{\rm EXT}$. The region $V_{\rm INT}$ is filled with an isotropic, linear, and possibly inhomogeneous material. Assuming that all fields and sources are time-harmonic, e.g., $\mathbf{E}(\mathbf{r},t) = \mathbf{E}(\mathbf{r})\exp(-{\rm i}\omega t)$, and that the host medium and the scatterer are nonmagnetic, it can be shown that the time-independent part of the electric field satisfies the volume integral equation (Saxon 1955b; Mishchenko et al. 2001)

$$\begin{aligned}\mathbf{E}(\mathbf{r}) &= \mathbf{E}^{\rm inc}(\mathbf{r}) + \mathbf{E}^{\rm sca}(\mathbf{r})\\ &= \mathbf{E}^{\rm inc}(\mathbf{r}) + {\rm k}_1^2 \int_{V_{\rm INT}} {\rm d}^3\mathbf{r}'\, \overleftrightarrow{G}(\mathbf{r},\mathbf{r}')\cdot\mathbf{E}(\mathbf{r}')[{\rm m}^2(\mathbf{r}')-1],\end{aligned} \tag{28}$$

where $\mathbf{r} \in V_{\rm INT} \cup V_{\rm EXT}$, $\mathbf{E}^{\rm inc}(\mathbf{r})$ is the incident field, ${\rm k}_1$ the wave number in the exterior region, ${\rm m}(\mathbf{r}) = {\rm m}_2(\mathbf{r})/{\rm m}_1 = {\rm k}_2(\mathbf{r})/{\rm k}_1$ the refractive index of the interior region relative to that of the exterior region, $\overleftrightarrow{G}(\mathbf{r},\mathbf{r}') = [\overleftrightarrow{I} + {\rm k}_1^{-2}\nabla\otimes\nabla]\times[\exp({\rm ik}_1|\mathbf{r}-\mathbf{r}'|)/4\pi|\mathbf{r}-\mathbf{r}'|]$ the free space dyadic Green's function, $\overleftrightarrow{I}$ the identity dyad, and $\otimes$ denotes a dyadic product of two vectors. This equation expresses the total electric field everywhere in space in terms of the incident field and the total field inside the scattering object. Since the latter is not known in general, one must solve (28) numerically or analytically. As a first step, the internal field can be approximated by the incident field. The resulting total field is substituted in the integral on the right-hand side of (28) in order to compute an improved approximation, and this iterative process is continued until the total field converges within a given numerical

accuracy. This procedure shows that the total electric field can be expressed in terms of the incident field as follows:

$$\mathbf{E}(\mathbf{r}) = \mathbf{E}^{\rm inc}(\mathbf{r}) + \int_{V_{\rm INT}} {\rm d}^3\mathbf{r}' \overleftrightarrow{G}(\mathbf{r},\mathbf{r}') \cdot \int_{V_{\rm INT}} {\rm d}^3\mathbf{r}'' \overleftrightarrow{T}(\mathbf{r}',\mathbf{r}'') \cdot \mathbf{E}^{\rm inc}(r''), \quad (29)$$

where $\overleftrightarrow{T}$ is the so-called dyad transition operator (Tsang et al. 1985).

Let us now choose an arbitrary point O close to the geometrical center of the scattering object as the common origin of all position vectors (Fig. 2). Usually one is interested in calculating the scattered field in the so-called far-field zone, i.e., assuming that ${\rm k}_1 r \gg 1$ and that r is much larger than the dimensions of the scattering object ($r \gg r'$). Since $|\mathbf{r}-\mathbf{r}'| = r[1-2\mathbf{r}'\cdot\hat{r}r^{-1} + r'^2r^{-2}]^{1/2} \underset{r\to\infty}{=} r - \mathbf{r}'\cdot\hat{r}$, where $\hat{r} = \mathbf{r}/r$ is the unit vector in the direction of $\mathbf{r}$, (28) yields

$$\mathbf{E}^{\rm sca}(\mathbf{r}) \underset{r\to\infty}{=} \frac{e^{{\rm i}{\rm k}_1 r}}{r}\frac{{\rm k}_1^2}{4\pi}(\overleftrightarrow{I} - \hat{r}\otimes\hat{r})\cdot\int_{\rm V_{INT}} {\rm d}^3\mathbf{r}'[{\rm m}^2(\mathbf{r}')-1]\mathbf{E}(\mathbf{r}')e^{-{\rm i}{\rm k}_1\mathbf{r}'\cdot\hat{r}}. \quad (30)$$

This important formula shows that the scattered field at a large distance from the object behaves as an outgoing transverse spherical wave. Indeed, the identity dyad in the spherical coordinate system centered at the origin is given by $\overleftrightarrow{I} = \hat{r}\otimes\hat{r} + \hat{\vartheta}\otimes\hat{\vartheta} + \hat{\varphi}\otimes\hat{\varphi}$. Therefore, the factor $\overleftrightarrow{I} - \hat{r}\otimes\hat{r} = \hat{\vartheta}\otimes\hat{\vartheta} + \hat{\varphi}\otimes\hat{\varphi}$ ensures that the scattered wave in the far-field zone is transverse: $\hat{r}\cdot\mathbf{E}^{\rm sca}(\mathbf{r}) \underset{r\to\infty}{=} 0$. Hence only the ϑ and φ components of the electric vector of the scattered field are nonzero. Furthermore, the scattered field decays inversely with distance r from the scattering object. Equation (30) can be rewritten as

$$\mathbf{E}^{\rm sca}(\mathbf{r}) \underset{r\to\infty}{=} \mathbf{E}_1^{\rm sca}(\hat{r})\,\exp({\rm i}{\rm k}_1 r)/r, \quad \hat{r}\cdot\mathbf{E}_1^{\rm sca}(\hat{r}) = 0, \quad (31)$$

where the vector $\mathbf{E}^{\rm sca}(\hat{r})$ is independent of r and describes the angular distribution of the scattered radiation in the far-field zone.

Assuming that the incident field is a plane electromagnetic wave given by

$$\mathbf{E}^{\rm inc}(\mathbf{r}) = \mathbf{E}_0^{\rm inc}\,\exp({\rm i}{\rm k}_1\hat{n}^{\rm inc}\cdot\mathbf{r}) \quad (32)$$

and using (29), we derive for the far-field zone

$$\mathbf{E}^{\rm sca}(\hat{n}^{\rm sca}r) \underset{r\to\infty}{=} r^{-1}\,\exp({\rm i}{\rm k}_1 r)\,\overleftrightarrow{A}(\hat{n}^{\rm sca},\hat{n}^{\rm inc})\cdot\mathbf{E}_0^{\rm inc}, \quad (33)$$

where $\hat{n}^{\rm sca} = \hat{r}$ and the scattering dyad $\overleftrightarrow{A}$ is given by

$$\begin{aligned}\overleftrightarrow{A}(\hat{n}^{\rm sca},\hat{n}^{\rm inc}) = (4\pi)^{-1}(\overleftrightarrow{I} - \hat{n}^{\rm sca}\otimes\hat{n}^{\rm sca})\cdot\textstyle\int_{V_{\rm INT}} {\rm d}^3\mathbf{r}'\,\exp(-{\rm i}{\rm k}_1\hat{n}^{\rm sca}\cdot\mathbf{r}')\\ \times\textstyle\int_{V_{\rm INT}} {\rm d}^3\mathbf{r}''\,\overleftrightarrow{T}(\mathbf{r}',\mathbf{r}'')\,\exp({\rm i}{\rm k}_1\hat{n}^{\rm inc}\cdot\mathbf{r}'').\end{aligned} \quad (34)$$

The elements of the scattering dyad have the dimension of length. It follows from (31) and (34) that $\hat{n}^{\rm sca}\cdot\overleftrightarrow{A}(\hat{n}^{\rm sca},\hat{n}^{\rm inc}) = 0$. Because the incident field given

by (32) is a transverse wave with electric vector perpendicular to the direction of propagation, the dot product $\overleftrightarrow{A}(\hat{n}^{\rm sca},\hat{n}^{\rm inc})\cdot\hat{n}^{\rm inc}$ is not defined by (33). We complete the definition by taking this product to be zero. As a consequence, only four components of the scattering dyad are independent. It is, therefore, convenient to formulate the scattering problem in the spherical coordinate system centered at the origin and introduce the so-called 2×2 amplitude matrix $\mathbf{S}$ which describes the transformation of the ϑ and φ components of the incident plane wave into the ϑ and φ components of the scattered spherical wave:

$$\begin{bmatrix} E_{\vartheta}^{\rm sca}(\hat{n}^{\rm sca}r) \\ E_{\varphi}^{\rm sca}(\hat{n}^{\rm sca}r) \end{bmatrix} \underset{r\to\infty}{=} \frac{e^{{\rm i}k_1 r}}{r}\mathbf{S}(\hat{n}^{\rm sca},\hat{n}^{\rm inc}) \begin{bmatrix} E_{0\vartheta}^{\rm inc} \\ E_{0\varphi}^{\rm inc} \end{bmatrix}. \tag{35}$$

The amplitude matrix depends on the directions of incidence and scattering as well as on the size, morphology, composition, and orientation of the scattering object with respect to the coordinate system. If known, the amplitude matrix provides the complete description of the scattering pattern in the far-field zone. The elements of the amplitude matrix have the dimension of length and are expressed in terms of the scattering dyad as follows:

$$\begin{aligned} S_{11} &= \hat{\vartheta}^{\rm sca}\cdot\overleftrightarrow{A}\cdot\hat{\vartheta}^{\rm inc}, \quad S_{12} = \hat{\vartheta}^{\rm sca}\cdot\overleftrightarrow{A}\cdot\hat{\varphi}^{\rm inc}, \\ S_{21} &= \hat{\varphi}^{\rm sca}\cdot\overleftrightarrow{A}\cdot\hat{\vartheta}^{\rm inc}, \quad S_{22} = \hat{\varphi}^{\rm sca}\cdot\overleftrightarrow{A}\cdot\hat{\varphi}^{\rm inc}. \end{aligned} \tag{36}$$

A fundamental property of the scattering dyad is the reciprocity relation, which is a manifestation of the symmetry of the scattering process with respect to an inversion of time (Saxon 1955a):

$$\overleftrightarrow{A}(-\hat{n}^{\rm inc},-\hat{n}^{\rm sca}) = \overleftrightarrow{A}^{\top}(\hat{n}^{\rm sca},\hat{n}^{\rm inc}). \tag{37}$$

The reciprocity relation for the amplitude matrix follows from (35) and (36) and the relations $\hat{\vartheta}(-\hat{n}) = \hat{\vartheta}(\hat{n})$ and $\hat{\varphi}(-\hat{n}) = -\hat{\varphi}(\hat{n})$:

$$\mathbf{S}(-\hat{n}^{\rm inc},-\hat{n}^{\rm sca}) = \begin{bmatrix} S_{11}(\hat{n}^{\rm sca},\hat{n}^{\rm inc}) & -S_{21}(\hat{n}^{\rm sca},\hat{n}^{\rm inc}) \\ -S_{12}(\hat{n}^{\rm sca},\hat{n}^{\rm inc}) & S_{22}(\hat{n}^{\rm sca},\hat{n}^{\rm inc}) \end{bmatrix}. \tag{38}$$

An important consequence of reciprocity is the so-called backscattering theorem, which directly follows from (37) (van de Hulst 1957):

$$S_{21}(-\hat{n},\hat{n}) = -S_{12}(-\hat{n},\hat{n}). \tag{39}$$

Although the knowledge of the amplitude matrix provides the complete description of the monochromatic scattering process in the far-field zone, the measurement of the amplitude matrix is a very complicated experimental problem involving the determination of both the amplitude and the phase of the incident and scattered waves. Measuring the phase is especially difficult, and only a handful of such experiments have been performed. The

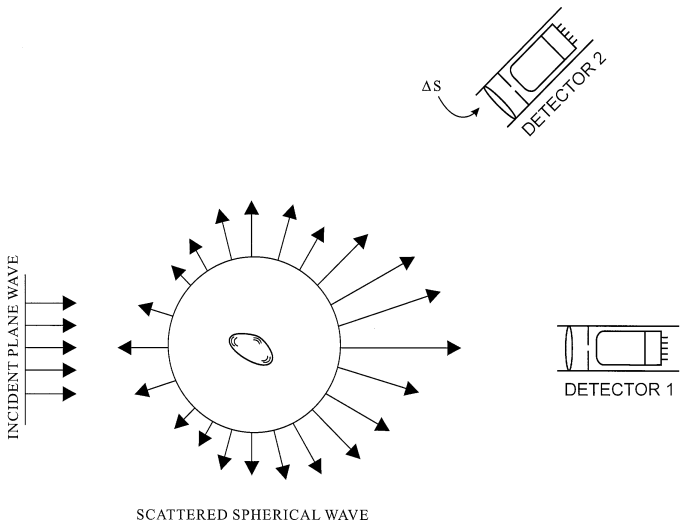

Fig. 3. Response of a collimated detector depends on the line of sight.

majority of other experiments have dealt with quasi-monochromatic rather than monochromatic light and involved measurements of derivative quantities having the dimension of energy flux rather than the electric field itself. It is, therefore, useful to characterize the scattering process using quantities that are easier to measure and are encountered more often, even though they may provide a less complete description of the scattering pattern in some cases.

Consider a collimated detector of electromagnetic radiation placed at a distance r from the particle in the far-field zone, with its surface ΔS aligned normal to and centered on $\mathbf{r}$ (Fig. 3). We assume that the dimension of the detector surface is much greater than any dimension of the scattering object but much smaller than r. It can be shown (van de Hulst 1957; Mishchenko et al. 2002) that the total electromagnetic power received by the detector is

$$W_{\Delta S}(\hat{r}) \approx \frac{1}{2}\sqrt{\varepsilon_1/\mu_0}\Delta S r^{-2}\left|\mathbf{E}_1^{\rm sca}(\hat{r})\right|^2 \tag{40}$$

when $\hat{r} \neq \hat{n}^{\rm inc}$ (detector 2), whereas for the exact forward direction (detector 1)

$$W_{\Delta S}(\hat{n}^{\rm inc}) \approx \sqrt{\varepsilon_1/\mu_0}\left[\frac{1}{2}\Delta S\left|\mathbf{E}_0^{\rm inc}\right|^2 - 2\pi \mathrm{k}_1^{-1}\mathrm{Im}\left[\mathbf{E}_1^{\rm sca}(\hat{n}^{\rm inc})\cdot\mathbf{E}_0^{\rm inc*}\right]\right] + O(r^{-2}). \tag{41}$$

The term $\frac{1}{2}\Delta S\sqrt{\varepsilon_1/\mu_0}\left|\mathbf{E}_0^{\rm inc}\right|$ on the right-hand side of (41) is proportional to the detector area ΔS and is equal to the electromagnetic power that would be received by detector 1 in the absence of the scattering particle, whereas $-\sqrt{\varepsilon_1/\mu_0}(2\pi/\mathrm{k}_1)\mathrm{Im}\left[\mathbf{E}_1^{\rm sca}(\hat{n}^{\rm inc})\cdot\mathbf{E}_0^{\rm inc*}\right]$ is an attenuation term independent

of ΔS and caused by interposing the particle in the incident wave. Thus, the well-collimated detector located in the far-field zone and having its surface aligned normal to the exact forward direction measures the power of the incident light attenuated by the interference of the incident and the scattered fields plus a negligibly small contribution from the scattered light, whereas the detector with surface aligned normal to any other scattering direction "sees" only the scattered light. These are two fundamental features of electromagnetic scattering by a small particle. Equation (41) is a representation of the so-called optical theorem.

The experiment schematically represented in Fig. 3 assumes that the detectors can measure only the total electromagnetic power and make no distinction between electromagnetic waves with different states of polarization. However, interposing a polarizer between the source of light and the scattering particle can generate incident light with a specific state of polarization, whereas interposing a polarizer between the scattering particle and the detector enables the measurement of the power corresponding to a particular polarization component of the scattered light. By repeating the measurement for different combinations of such polarizers, one can determine the law describing the transformation of a complete set of polarization characteristics of the incident light into that of the scattered light provided that both sets of characteristics have the same dimension of energy flux.

To derive the relationship between the polarization characteristics of the incident and the scattered waves for scattering directions away from the incidence direction ($\hat{r} \neq \hat{n}^{\rm inc}$), we first define the respective Stokes parameters:

$$\mathbf{I}^{\rm inc} = \frac{1}{2}\sqrt{\frac{\varepsilon_1}{\mu_0}} \begin{bmatrix} E_{0\vartheta}^{\rm inc} E_{0\vartheta}^{\rm inc*} + E_{0\varphi}^{\rm inc} E_{0\varphi}^{\rm inc*} \\ E_{0\vartheta}^{\rm inc} E_{0\vartheta}^{\rm inc*} - E_{0\varphi}^{\rm inc} E_{0\varphi}^{\rm inc*} \\ -E_{0\vartheta}^{\rm inc} E_{0\varphi}^{\rm inc*} - E_{0\varphi}^{\rm inc} E_{0\vartheta}^{\rm inc*} \\ {\rm i}(E_{0\varphi}^{\rm inc} E_{0\vartheta}^{\rm inc*} - E_{0\vartheta}^{\rm inc} E_{0\varphi}^{\rm inc*}) \end{bmatrix}, \tag{42}$$

$$\mathbf{I}^{\rm sca} = \frac{1}{r^2}\frac{1}{2}\sqrt{\frac{\varepsilon_1}{\mu_0}} \begin{bmatrix} E_{1\vartheta}^{\rm sca} E_{1\vartheta}^{\rm sca*} + E_{1\varphi}^{\rm sca} E_{1\varphi}^{\rm sca*} \\ E_{1\vartheta}^{\rm sca} E_{1\vartheta}^{\rm sca*} - E_{1\varphi}^{\rm sca} E_{1\varphi}^{\rm sca*} \\ -E_{1\vartheta}^{\rm sca} E_{1\varphi}^{\rm sca*} - E_{1\varphi}^{\rm sca} E_{1\vartheta}^{\rm sca*} \\ {\rm i}(E_{1\varphi}^{\rm sca} E_{1\vartheta}^{\rm sca*} - E_{1\vartheta}^{\rm sca} E_{1\varphi}^{\rm sca*}) \end{bmatrix}. \tag{43}$$

We then derive

$$\mathbf{I}^{\rm sca}(r\hat{n}^{\rm sca}) = r^{-2}\mathbf{Z}(\hat{n}^{\rm sca}, \hat{n}^{\rm inc})\mathbf{I}^{\rm inc}, \tag{44}$$

where the phase matrix $\mathbf{Z}$ describes the transformation of the Stokes vector of the incident wave into that of the scattered wave. The explicit formulas for the elements of the phase matrix in terms of the amplitude matrix are as follows:

$$\mathrm{Z}_{11} = \frac{1}{2}\left(|S_{11}|^2 + |S_{12}|^2 + |S_{21}|^2 + |S_{22}|^2\right), \tag{45}$$

$$\mathrm{Z}_{12} = \frac{1}{2}\left(|S_{11}|^2 - |S_{12}|^2 + |S_{21}|^2 - |S_{22}|^2\right), \tag{46}$$

$$\mathrm{Z}_{13} = -\mathrm{Re}\left(S_{11}S_{12}^* + S_{22}S_{21}^*\right), \tag{47}$$

$$\mathrm{Z}_{14} = -\mathrm{Im}\left(S_{11}S_{12}^* - S_{22}S_{21}^*\right), \tag{48}$$

$$\mathrm{Z}_{21} = \frac{1}{2}\left(|S_{11}|^2 + |S_{12}|^2 - |S_{21}|^2 - |S_{22}|^2\right), \tag{49}$$

$$\mathrm{Z}_{22} = \frac{1}{2}\left(|S_{11}|^2 - |S_{12}|^2 - |S_{21}|^2 + |S_{22}|^2\right), \tag{50}$$

$$\mathrm{Z}_{23} = -\mathrm{Re}\left(S_{11}S_{12}^* - S_{22}S_{21}^*\right), \tag{51}$$

$$\mathrm{Z}_{24} = -\mathrm{Im}\left(S_{11}S_{12}^* + S_{22}S_{21}^*\right), \tag{52}$$

$$\mathrm{Z}_{31} = -\mathrm{Re}\left(S_{11}S_{21}^* + S_{22}S_{12}^*\right), \tag{53}$$

$$\mathrm{Z}_{32} = -\mathrm{Re}\left(S_{11}S_{21}^* - S_{22}S_{12}^*\right), \tag{54}$$

$$\mathrm{Z}_{33} = \mathrm{Re}\left(S_{11}S_{22}^* + S_{12}S_{21}^*\right), \tag{55}$$

$$\mathrm{Z}_{34} = \mathrm{Im}\left(S_{11}S_{22}^* + S_{21}S_{12}^*\right), \tag{56}$$

$$\mathrm{Z}_{41} = -\mathrm{Im}\left(S_{21}S_{11}^* + S_{22}S_{12}^*\right), \tag{57}$$

$$\mathrm{Z}_{42} = -\mathrm{Im}\left(S_{21}S_{11}^* - S_{22}S_{12}^*\right), \tag{58}$$

$$\mathrm{Z}_{43} = \mathrm{Im}\left(S_{22}S_{11}^* - S_{12}S_{21}^*\right), \tag{59}$$

$$\mathrm{Z}_{44} = \mathrm{Re}\left(S_{22}S_{11}^* - S_{12}S_{21}^*\right) \ . \tag{60}$$

Up to this point we have considered only scattering of monochromatic plane waves. However, (44) remains valid even when the incident radiation is a parallel quasi-monochromatic beam of light provided that the Stokes vectors entering this equation are averages over a time interval long compared with the period of fluctuations. This explains the usefulness of the phase matrix concept in situations involving quasi-monochromatic light.

In general, all 16 elements of the phase matrix are nonzero. However, the phase matrix elements for a single particle are expressed in terms of only seven independent real numbers resulting from the four moduli $|S_{ij}|\,(i,j=1,2)$ and three differences in phase between S_{ij}. Therefore, only seven of the phase matrix elements are independent, and there must be nine independent relations among the 16 phase matrix elements. Furthermore, the specific mathematical structure of the phase matrix can also be used to derive many useful linear and quadratic inequalities for the phase matrix elements. Two most important inequalities are $Z_{11} \geq 0$ and $|Z_{ij}| \leq Z_{11}(i,j=1,\ldots,4)$. The reader is referred to Hovenier and van der Mee (2000) for a review of this subject and a discussion of how the general properties of the phase matrix can be used for testing the results of theoretical computations and laboratory measurements. From (38) and (45)–(60) we derive the reciprocity relation for the phase matrix:

$$\mathbf{Z}(-\hat{n}^{\rm inc},-\hat{n}^{\rm sca})=\mathbf{\Delta}_3\mathbf{Z}^{\top}(\hat{n}^{\rm sca},\hat{n}^{\rm inc})\mathbf{\Delta}_3, \tag{61}$$

where $\mathbf{\Delta}_3=\mathrm{diag}[1,1,-1,1]$. The backscattering theorem, (39), leads to the following property of the backscattering phase matrix (Mishchenko et al. 2000b):

$$Z_{11}(-\hat{n},\hat{n})-Z_{22}(-\hat{n},\hat{n})+Z_{33}(-\hat{n},\hat{n})-Z_{44}(-\hat{n},\hat{n})=0\,. \tag{62}$$

Electromagnetic scattering most typically produces light with polarization characteristics different from those of the incident beam. If the incident beam is unpolarized, i.e., $\mathbf{I}^{\rm inc}=(I^{\rm inc},0,0,0)^{\top}$, the scattered light generally has at least one nonzero Stokes parameter other than intensity:

$$I^{\rm sca}=Z_{11}I^{\rm inc},\quad Q^{\rm sca}=Z_{21}I^{\rm inc},\quad U^{\rm sca}=Z_{31}I^{\rm inc},\quad V^{\rm sca}=Z_{41}I^{\rm inc}. \tag{63}$$

This phenomenon is traditionally called "polarization" and results in scattered light with finite degree of polarization: $P=\sqrt{Z_{21}^2+Z_{31}^2+Z_{41}^2}/Z_{11}$. If the incident light is unpolarized, then the element Z_{11} determines the angular distribution of the scattered intensity. When the incident beam is linearly polarized, i.e., $\mathbf{I}^{\rm inc}=(I^{\rm inc},Q^{\rm inc},U^{\rm inc},0)^{\top}$, the scattered light may become elliptically polarized ($V^{\rm sca}\neq 0$). Conversely, when the incident light is circularly polarized, i.e., $\mathbf{I}^{\rm inc}=(I^{\rm inc},0,0,V^{\rm inc})^{\top}$, the scattered light may become partially linearly polarized ($Q^{\rm sca}\neq 0$ and/or $U^{\rm sca}\neq 0$).

Let us now consider the exact forward-scattering direction ($\hat{r}=\hat{n}^{\rm inc}$). We begin by defining the Stokes vector of the total field for $\hat{r}$ close to $\hat{n}^{\rm inc}$ as

$$\mathbf{I}=\frac{1}{2}\sqrt{\frac{\varepsilon_1}{\mu_0}}\begin{bmatrix}E_\vartheta E_\vartheta^*+E_\varphi E_\varphi^*\\ E_\vartheta E_\vartheta^*-E_\varphi E_\varphi^*\\ -E_\vartheta E_\varphi^*-E_\varphi E_\vartheta^*\\ \mathrm{i}(E_\varphi E_\vartheta^*-E_\vartheta E_\varphi^*)\end{bmatrix}, \tag{64}$$

where the total electric field is

$$\mathbf{E}(r\hat{r})=\mathbf{E}^{\rm inc}(r\hat{r})+\mathbf{E}^{\rm sca}(r\hat{r})\,. \tag{65}$$

Integrating the elements of $\mathbf{I}(r\hat{r})$ over the surface of the collimated detector aligned normal to $\hat{n}^{\rm inc}$, one can derive

$$\mathbf{I}(r\hat{n}^{\rm inc})\Delta S=\mathbf{I}^{\rm inc}\Delta S-\mathbf{K}(\hat{n}^{\rm inc})\mathbf{I}^{\rm inc}+O(r^{-2}), \tag{66}$$

where $\mathbf{K}(\hat{n}^{\rm inc})$ is the so-called extinction matrix. The elements of $\mathbf{K}(\hat{n}^{\rm inc})$ have the dimension of area and are expressed in the elements of the forward-scattering amplitude matrix $\mathbf{S}(\hat{n}^{\rm inc},\hat{n}^{\rm inc})$ as follows (Mishchenko et al. 2000b, 2002):

$$\mathrm{K}_{jj} = (2\pi/\mathrm{k}_1)\,\mathrm{Im}\,[S_{11} + S_{22}] \quad j = 1, ..., 4, \tag{67}$$

$$\mathrm{K}_{12} = \mathrm{K}_{21} = (2\pi/\mathrm{k}_1)\,\mathrm{Im}\,[S_{11} - S_{22}], \tag{68}$$

$$\mathrm{K}_{13} = \mathrm{K}_{31} = -(2\pi/\mathrm{k}_1)\,\mathrm{Im}\,[S_{12} + S_{21}], \tag{69}$$

$$\mathrm{K}_{14} = \mathrm{K}_{41} = (2\pi/\mathrm{k}_1)\,\mathrm{Re}\,[S_{21} - S_{12}], \tag{70}$$

$$\mathrm{K}_{23} = -\mathrm{K}_{32} = (2\pi/\mathrm{k}_1)\,\mathrm{Im}\,[S_{21} - S_{12}], \tag{71}$$

$$\mathrm{K}_{24} = -\mathrm{K}_{42} = -(2\pi/\mathrm{k}_1)\,\mathrm{Re}\,[S_{12} + S_{21}], \tag{72}$$

$$\mathrm{K}_{34} = -\mathrm{K}_{43} = (2\pi/\mathrm{k}_1)\,\mathrm{Re}\,[S_{22} - S_{11}]. \tag{73}$$

Equation (66) represents the most general form of the optical theorem. It shows that the presence of the scattering particle changes not only the total power of the electromagnetic radiation received by the detector facing the incident wave (detector 1 in Fig. 3), but also its state of polarization. This phenomenon is called dichroism and results from different attenuation rates for different polarization components of the incident wave. Equation (66) remains valid when the incident radiation is a parallel quasi-monochromatic beam of light rather than a monochromatic plane wave. From (38) and (67)–(73) we obtain the reciprocity relation

$$\mathbf{K}(-\hat{n}^{\mathrm{inc}}) = \mathbf{\Delta}_3\mathbf{K}^{\top}(\hat{n}^{\mathrm{inc}})\mathbf{\Delta}_3. \tag{74}$$

The knowledge of the total electromagnetic field in the far-field zone also allows us to calculate the total scattering, absorption, and extinction cross sections defined as follows. The product of the scattering cross section C_{sca} and the incident monochromatic energy flux gives the total monochromatic power removed from the incident wave resulting solely from scattering of the incident radiation in all directions. Analogously, the product of the absorption cross section C_{abs} and the incident monochromatic energy flux gives the total monochromatic power removed from the incident wave as a result of absorption of light by the object. Of course, the absorbed electromagnetic energy does not disappear, but rather is converted into other forms of energy. Finally, the extinction cross section C_{ext} is the sum of the scattering and absorption cross sections and, when multiplied by the incident monochromatic energy flux, gives the total monochromatic power removed from the incident light due to the combined effect of scattering and absorption.

In view of (44) and (66), the extinction and scattering cross sections are given by

$$\begin{aligned} C_{\mathrm{ext}} = {} & \frac{1}{I^{\mathrm{inc}}}[\mathrm{K}_{11}(\hat{n}^{\mathrm{inc}})I^{\mathrm{inc}} + \mathrm{K}_{12}(\hat{n}^{\mathrm{inc}})Q^{\mathrm{inc}} \\ & + \mathrm{K}_{13}(\hat{n}^{\mathrm{inc}})U^{\mathrm{inc}} + \mathrm{K}_{14}(\hat{n}^{\mathrm{inc}})V^{\mathrm{inc}}], \end{aligned} \tag{75}$$

$$\begin{aligned} C_{\mathrm{sca}} = {} & \frac{1}{I^{\mathrm{inc}}}\int_{4\pi} \mathrm{d}\hat{r}[Z_{11}(\hat{r}, \hat{n}^{\mathrm{inc}})I^{\mathrm{inc}} + Z_{12}(\hat{r}, \hat{n}^{\mathrm{inc}})Q^{\mathrm{inc}} \\ & + Z_{13}(\hat{r}, \hat{n}^{\mathrm{inc}})U^{\mathrm{inc}} + Z_{14}(\hat{r}, \hat{n}^{\mathrm{inc}})V^{\mathrm{inc}}]. \end{aligned} \tag{76}$$

The absorption cross section is equal to the difference of the extinction and scattering cross sections:

$$C_{\rm abs} = C_{\rm ext} - C_{\rm sca} \geq 0. \tag{77}$$

The single-scattering albedo is defined as the ratio of the scattering and extinction cross sections:

$$\varpi = C_{\rm sca}/C_{\rm ext} \leq 1\,. \tag{78}$$

This quantity is widely used in the radiative transfer theory (see, e.g., the chapter by Stamnes) and is interpreted as the probability that a photon interacting with the particle will be scattered rather than absorbed. Obviously, $\varpi = 1$ for nonabsorbing particles. Equations (75)–(78) also hold for quasi-monochromatic incident light provided that the elements of the Stokes vector are averages over a time interval long compared with the period of fluctuations. All cross sections are inherently positive quantities and have the dimension of area. They depend on the direction, polarization state, and wavelength of the incident light as well as on the particle size, morphology, refractive index, and orientation with respect to the reference frame.

If the particle absolute temperature T is above zero, it can emit as well as scatter and absorb electromagnetic radiation. The emitted radiation in the far-field zone of the particle propagates in the radial direction, i.e., along the unit vector $\hat{n} = \mathbf{r}/r$, where $\mathbf{r}$ is the position vector of the observation point with origin inside the particle. The energetic and polarization characteristics of the emitted radiation are described by a 4-component emission column vector $\mathbf{K}_{\rm e}(\hat{n}, T, \omega)$ defined such that the net rate at which the emitted energy crosses a surface element ΔS normal to $\hat{n}$ at a distance r from the particle at frequencies from ω to $\omega + \Delta\omega$ is

$$W^{\rm e} = \frac{1}{r^2}{\rm K}_{\rm el}(\hat{n}, T, \omega)\Delta S \Delta\omega. \tag{79}$$

The emission vector can be expressed in terms of the extinction and phase matrices as follows (Mishchenko et al. 2000b, 2002):

$${\rm K}_{{\rm e}i}(\hat{n}, T, \omega) = I_{\rm b}(T, \omega){\rm K}_{i1}(\hat{n}, \omega) - I_{\rm b}(T, \omega)\int_{4\pi} {\rm d}\hat{n}' Z_{i1}(\hat{n}, \hat{n}', \omega), i = 1, ..., 4, \tag{80}$$

where $I_{\rm b}(T, \omega) = \hbar\omega^3/\{4\pi^3 c^2[\exp(\hbar\omega/k_{\rm B}T) - 1]\}$ is the Planck energy distribution function, $\hbar = h/2\pi$, h is Planck's constant, c is the speed of light in a vacuum, and $k_{\rm B}$ is Boltzmann's constant.

4 Scattering, Absorption, and Emission by a Collection of Independently Scattering Particles

The formalism developed in the previous section strictly applies only to scattering of monochromatic or quasi-monochromatic light by an isolated particle

in the form of a single body or a finite aggregate (Fig. 2). However, it can also be applied to single scattering by collections of independently scattering particles under certain simplifying assumptions.

Consider first a small volume element having a linear dimension l and comprising a number N of randomly positioned particles and illuminated by a plane electromagnetic wave. Although the volume element is assumed to be macroscopically small, its linear dimension must still be much larger than the size of the particles and the wavelength of the incident light. We assume that N is small enough so that the mean distance between the particles is also much larger than the incident wavelength and the average particle size. This means that each particle is located in the far-field zone of all other particles and scatters the incident light in exactly the same way as if all other particles did not exist. We also assume that N is sufficiently small so that the main contribution to the total scattered radiation exiting the volume element comes from light scattered only once. In other words, the contribution of light scattered two and more times by particles inside the volume element is assumed to be negligibly small. This is equivalent to requiring that the "optical size" $N\langle C_{\rm sca}\rangle l^{-2}$ of the volume element be much smaller than one, where $\langle C_{\rm sca}\rangle$ is the average scattering cross section per particle. Finally, we assume that the positions of the particles are sufficiently random so that there are no systematic phase relations between individual waves scattered by different particles. It can then be shown that the total optical characteristics of the volume element are given by

$$C_{\rm sca} = \sum_{n=1}^{N} (C_{\rm sca})_n = N\langle C_{\rm sca}\rangle, \tag{81}$$

$$C_{\rm ext} = \sum (C_{\rm ext})_n = N\langle C_{\rm ext}\rangle, \tag{82}$$

$$C_{\rm abs} = \sum (C_{\rm abs})_n = N\langle C_{\rm abs}\rangle, \tag{83}$$

$$\mathbf{Z} = \sum \mathbf{Z}_n = N\langle \mathbf{Z}\rangle, \tag{84}$$

$$\mathbf{K} = \sum \mathbf{K}_n = N\langle \mathbf{K}\rangle, \tag{85}$$

$$\mathbf{K}_{\rm e} = \sum (\mathbf{K}_{\rm e})_n = N\langle \mathbf{K}_{\rm e}\rangle, \tag{86}$$

where n numbers the particles and $\langle C_{\rm sca}\rangle$, $\langle C_{\rm ext}\rangle$, $\langle C_{\rm abs}\rangle$, $\langle \mathbf{Z}\rangle$, $\langle \mathbf{K}\rangle$, and $\langle \mathbf{K}_{\rm e}\rangle$ are the average scattering, extinction, and absorption cross sections, the phase and extinction matrices, and the emission vector per particle, respectively. Thus, the optical cross sections and the phase and extinction matrices of the small volume element comprising randomly positioned, widely separated particles are obtained by adding the respective optical characteristics of the individual particles. Obviously, this property of additivity also holds when the incident light is a parallel quasi-monochromatic beam rather than a plane electromagnetic wave.

It is not always easy to determine what minimal interparticle separation allows the use of the concept of the single-particle amplitude matrix and makes particles independent scatterers. Exact calculations for randomly oriented two-sphere clusters composed of wavelength-sized spheres suggest that particles can scatter independently when the distance between their centers is as small as four times their radius (Mishchenko et al. 1995). Even though this result is not necessarily a universal rule and may be expected to become inapplicable for subwavelength-sized particles, it can be considered a simple approximate condition of independent scattering by particles comparable to and larger than a wavelength.

Scattering media encountered in practice are usually mixtures of particles with different sizes, shapes, orientations, and refractive indices. Equations (81)–(86) imply that theoretical computations of single light scattering, absorption, and emission by a small volume element consisting of such particles must include averaging the optical cross sections, the phase and extinction matrices, and the emission vector over a representative particle ensemble. The computation of ensemble averages is, in principle, rather straightforward and involves numerical integration over a distribution of particle sizes, shapes, refractive indices, and/or orientations (Mishchenko et al. 2000b).

The quantities introduced above can also be used to describe multiple scattering by a large collection of independent particles. The general radiative transfer equation for an emitting medium comprising sparsely and randomly distributed, arbitrarily oriented nonspherical particles is as follows (Tsang et al. 1985; Mishchenko 2002):

$$\mathrm{d}\mathbf{I}(\hat{n},\omega)/\mathrm{d}s = -n_0\langle\mathbf{K}(\hat{n},\omega)\rangle\mathbf{I}(\hat{n},\omega) + n_0\langle\mathbf{K}_{\mathrm{e}}(\hat{n},T,\omega)\rangle + n_0\int_{4\pi}\mathrm{d}\hat{n}'\langle\mathbf{Z}(\hat{n},\hat{n}',\omega)\rangle\mathbf{I}(\hat{n}',\omega), \tag{87}$$

where the four-component column vector $\mathbf{I}$ is the specific intensity vector of multiply scattered light propagating in the direction $\hat{n}$, the pathlength element $\mathrm{d}s$ is measured along $\hat{n}$, and n_0 is the particle number density. The first term on the right-hand side of (87) describes the change of the specific intensity vector due to extinction, the second term describes the contribution of the emitted light, and the third term is the contribution of light illuminating a small volume element from all directions $\hat{n}'$ and scattered in the direction $\hat{n}$. It is important to recognize that although we use the same symbol $\mathbf{I}$ to denote the Stokes vector of a transverse electromagnetic wave in (23) and the specific intensity vector in (87), their dimensions are different: the elements of the Stokes vector have the dimension of monochromatic energy flux, whereas those of the specific intensity vector have the dimension of monochromatic radiance (energy per unit area per unit time per unit wavelength per unit solid angle). The radiative transfer equation must be supplemented by boundary conditions appropriate for a particular physical problem. For example, the standard model of a planetary atmosphere is a plane-parallel system illuminated from above by solar radiation (see the chapter by Stamnes).

5 Isotropic and Symmetric Scattering Media

By definition, the phase matrix relates the Stokes parameters of the incident and scattered beams defined relative to their respective meridional planes. Unlike the phase matrix, the scattering matrix $\mathbf{F}$ relates the Stokes parameters of the incident and scattered beams defined with respect to the scattering plane, that is, the plane through $\hat{n}^{\rm inc}$ and $\hat{n}^{\rm sca}$ (van de Hulst 1957). A simple way to introduce the scattering matrix is to direct the z axis of the reference frame along the incident beam and superpose the meridional plane with $\varphi^{\rm sca} = \varphi^{\rm inc} = 0$ with the scattering plane (Fig. 1). Then the scattering matrix $\mathbf{F}$ can be defined as

$$\mathbf{F}(\vartheta^{\rm sca}) = \mathbf{Z}(\vartheta^{\rm sca}, \varphi^{\rm sca} = 0;\ \vartheta^{\rm inc} = 0, \varphi^{\rm inc} = 0). \tag{88}$$

In general, all 16 elements of the scattering matrix are nonzero and depend on the particle orientation with respect to the incident and scattered beams.

The choice of the laboratory reference frame having the xz plane coinciding with the scattering plane can often be inconvenient because any change in the orientation of the scattering plane then also changes the orientation of the scattering particle with respect to the coordinate system. However, the concept of scattering matrix can be very useful in application to so-called macroscopically isotropic and mirror symmetric scattering media, because in this case the scattering matrix of a particle collection becomes independent of the incidence direction and the orientation of the scattering plane, is functionally dependent only on the angle $\Theta = \cos^{-1}(\hat{n}^{\rm inc} \cdot \hat{n}^{\rm sca})$ between the incident and scattered beams, and has a simple block-diagonal structure (van de Hulst 1957):

$$\mathbf{F}(\Theta) = \begin{bmatrix} F_{11}(\Theta) & F_{12}(\Theta) & 0 & 0 \\ F_{12}(\Theta) & F_{22}(\Theta) & 0 & 0 \\ 0 & 0 & F_{33}(\Theta) & F_{34}(\Theta) \\ 0 & 0 & -F_{34}(\Theta) & F_{44}(\Theta) \end{bmatrix} = N\langle \mathbf{F}(\Theta) \rangle, \tag{89}$$

where N is the number of particles in the volume element and $\langle \mathbf{F}(\Theta) \rangle$ is the ensemble-averaged scattering matrix per particle. By definition, the scattering medium is *macroscopically isotropic and mirror symmetric* if it is composed of randomly oriented particles with a plane of symmetry and/or equal numbers of randomly oriented particles and their mirror-symmetric counterparts.

The knowledge of the matrix $\mathbf{F}(\Theta)$ can be used to calculate the Stokes phase matrix for an isotropic and symmetric scattering medium. Assume that $0 < \varphi^{\rm sca} - \varphi^{\rm inc} < \pi$ and consider the phase matrix $\mathbf{Z}(\vartheta^{\rm sca}, \varphi^{\rm sca}; \vartheta^{\rm inc}, \varphi^{\rm inc})$ (Fig. 4). The phase matrix links the Stokes vectors of the incident and scattered beams specified relative to their respective meridional planes. Therefore, to compute the Stokes vector of the scattered beam with respect to its

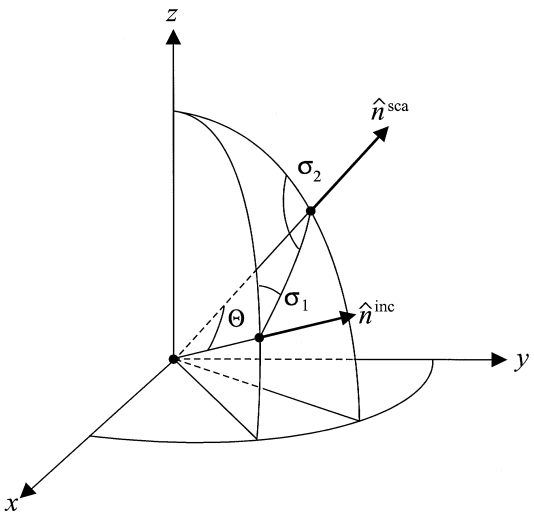

Fig. 4. On the relationship between scattering and phase matrices.

meridional plane, we must (i) calculate the Stokes vector of the incident beam with respect to the scattering plane; (ii) multiply it by the scattering matrix, thereby obtaining the Stokes vector of the scattered beam with respect to the scattering plane; and finally (iii) compute the Stokes vector of the scattered beam with respect to its meridional plane. This procedure yields

$$\mathbf{Z}(\vartheta^{\rm sca},\varphi^{\rm sca};\vartheta^{\rm inc},\varphi^{\rm inc}) = \mathbf{L}(-\sigma_2)\mathbf{F}(\Theta)\mathbf{L}(\pi-\sigma_1), \tag{90}$$

where

$$\mathbf{L}(\eta) = \begin{bmatrix} 1 & 0 & 0 & 0 \\ 0 & \cos 2\eta & -\sin 2\eta & 0 \\ 0 & \sin 2\eta & \cos 2\eta & 0 \\ 0 & 0 & 0 & 1 \end{bmatrix} \tag{91}$$

is the rotation matrix which describes the transformation of the Stokes parameters when the reference plane is rotated about the direction of propagation through an angle $0 \leq \eta < 2\pi$ in the *clockwise* direction when looking in the direction of propagation. The scattering angle Θ and the rotation angles σ_1 and σ_2 can be calculated from $\vartheta^{\rm sca}, \vartheta^{\rm inc}, \varphi^{\rm sca}$, and $\varphi^{\rm inc}$ using spherical trigonometry:

$$\cos\Theta = \cos\vartheta^{\rm sca}\cos\vartheta^{\rm inc} + \sin\vartheta^{\rm sca}\sin\vartheta^{\rm inc}\cos(\varphi^{\rm sca}-\varphi^{\rm inc})\,, \tag{92}$$

$$\cos\sigma_1 = \frac{\cos\vartheta^{\rm sca} - \cos\vartheta^{\rm inc}\cos\Theta}{\sin\vartheta^{\rm inc}\sin\Theta}\,, \tag{93}$$

$$\cos\sigma_2 = \frac{\cos\vartheta^{\rm inc} - \cos\vartheta^{\rm sca}\cos\Theta}{\sin\vartheta^{\rm sca}\sin\Theta}\,. \tag{94}$$

Equations (90) and (92)–(94) demonstrate that the phase matrix of a macroscopically isotropic and symmetric medium depends only on the difference of the azimuthal angles of the scattered and incident beams rather than on their specific values. This matrix satisfies the symmetry relations (Hovenier and van der Mee 1983)

$$\mathbf{Z}(\vartheta^{\rm sca},\varphi^{\rm inc};\vartheta^{\rm inc},\varphi^{\rm sca}) = \mathbf{\Delta}_{34}\mathbf{Z}(\vartheta^{\rm sca},\varphi^{\rm sca};\vartheta^{\rm inc},\varphi^{\rm inc})\mathbf{\Delta}_{34}, \quad (95)$$

$$\mathbf{Z}(\pi-\vartheta^{\rm sca},\varphi^{\rm sca};\pi-\vartheta^{\rm inc},\varphi^{\rm inc}) = \mathbf{\Delta}_{34}\mathbf{Z}(\vartheta^{\rm sca},\varphi^{\rm sca};\vartheta^{\rm inc},\varphi^{\rm inc})\mathbf{\Delta}_{34}, \quad (96)$$

where $\mathbf{\Delta}_{34} = {\rm diag}[1,1,-1,-1]$. Although (90) is valid for $0 < \varphi^{\rm sca} - \varphi^{\rm inc} < \pi$, combining it with (95) yields the phase matrix for all possible incidence and scattering directions.

The extinction matrix for an isotropic and symmetric scattering medium is direction-independent and diagonal:

$$\mathbf{K}(\hat{n}) \equiv \mathbf{K} = C_{\rm ext}\mathbf{\Delta} = N\langle C_{\rm ext}\rangle\mathbf{\Delta}, \quad (97)$$

where $\mathbf{\Delta}$ is the 4×4 unit matrix, N is the number of particles in the volume element, and $\langle C_{\rm ext}\rangle$ is the average extinction cross section per particle. The latter is now independent of the polarization state of the incident light. The average scattering cross section per particle is also independent of the direction of propagation and polarization state of the incident light and is given by

$$\langle C_{\rm sca}\rangle = 2\pi\int_0^\pi {\rm d}\vartheta\langle F_{11}(\vartheta)\rangle. \quad (98)$$

The average absorption cross section per particle,

$$\langle C_{\rm abs}\rangle = \langle C_{\rm ext}\rangle - \langle C_{\rm sca}\rangle, \quad (99)$$

and the average single-scattering albedo,

$$\varpi = \langle C_{\rm sca}\rangle/\langle C_{\rm ext}\rangle, \quad (100)$$

are also independent of the direction and polarization of the incident beam. The same is true of the extinction, scattering, and absorption efficiency factors defined as

$$Q_{\rm ext} = \langle C_{\rm ext}\rangle/\langle G\rangle, \quad Q_{\rm sca} = \langle C_{\rm sca}\rangle/\langle G\rangle, \quad Q_{\rm abs} = \langle C_{\rm abs}\rangle/\langle G\rangle, \quad (101)$$

respectively, where $\langle G\rangle$ is the average projection area per particle. The ensemble-averaged emission vector per particle is given by

$$\langle \mathbf{K}_{\rm e}(\hat{n},T,\omega)\rangle \equiv \langle \mathbf{K}_{\rm e}(T,\omega)\rangle = \langle C_{\rm abs}\rangle[I_{\rm b}(T,\omega),0,0,0]^\top, \quad (102)$$

where $\langle C_{\rm abs}\rangle$ may depend on frequency. Thus, radiation emitted by a small volume element comprising equal numbers of randomly oriented particles and

their mirror-symmetric counterparts and/or randomly oriented particles with a plane of symmetry is isotropic and unpolarized.

The scattering matrix simplifies when $\Theta = 0$ or $\Theta = \pi$ (van de Hulst 1957; Mishchenko and Hovenier 1995):

$$\mathbf{F}(0) = \mathrm{diag}\{F_{11}(0), F_{22}(0), F_{22}(0), F_{44}(0)\}, \tag{103}$$

$$\mathbf{F}(\pi) = \mathrm{diag}\{F_{11}(\pi), F_{22}(\pi), -F_{22}(\pi), F_{11}(\pi) - 2F_{22}(\pi)\}. \tag{104}$$

The structure of the scattering matrix becomes especially simple for spherically symmetric particles:

$$\mathbf{F}(\Theta) = \begin{bmatrix} F_{11}(\Theta) & F_{12}(\Theta) & 0 & 0 \\ F_{12}(\Theta) & F_{11}(\Theta) & 0 & 0 \\ 0 & 0 & F_{33}(\Theta) & F_{34}(\Theta) \\ 0 & 0 & -F_{34}(\Theta) & F_{33}(\Theta) \end{bmatrix}. \tag{105}$$

The scattering matrix of this type will be referred to as the Lorenz–Mie scattering matrix. In this case (103) and (104) imply that $F_{33}(0) = F_{11}(0)$ and $F_{33}(\pi) = -F_{11}(\pi)$.

It is convenient and customary in many types of applications to use the so-called normalized scattering matrix

$$\widetilde{\mathbf{F}}(\Theta) = \frac{4\pi}{\langle C_{\mathrm{sca}} \rangle} \langle \mathbf{F}(\Theta) \rangle = \begin{bmatrix} a_1(\Theta) & b_1(\Theta) & 0 & 0 \\ b_1(\Theta) & a_2(\Theta) & 0 & 0 \\ 0 & 0 & a_3(\Theta) & b_2(\Theta) \\ 0 & 0 & -b_2(\Theta) & a_4(\Theta) \end{bmatrix} \tag{106}$$

with dimensionless elements. Similarly, the normalized phase matrix can be defined as

$$\widetilde{\mathbf{Z}}(\vartheta^{\mathrm{sca}}, \varphi^{\mathrm{sca}}; \vartheta^{\mathrm{inc}}, \varphi^{\mathrm{inc}}) = \frac{4\pi}{\langle C_{\mathrm{sca}} \rangle} \langle \mathbf{Z}(\vartheta^{\mathrm{sca}}, \varphi^{\mathrm{sca}}; \vartheta^{\mathrm{inc}}, \varphi^{\mathrm{inc}}) \rangle. \tag{107}$$

The (1,1) element of the normalized scattering matrix, $a_1(\Theta)$, is traditionally called the phase function and, as follows from (98) and (106), satisfies the normalization condition

$$\frac{1}{2} \int_0^\pi \mathrm{d}\Theta \sin\Theta a_1(\Theta) = 1. \tag{108}$$

The asymmetry parameter is defined as

$$\langle \cos\Theta \rangle = \frac{1}{2} \int_0^\pi \mathrm{d}\Theta \sin\Theta a_1(\Theta) \cos\Theta. \tag{109}$$

The asymmetry parameter is positive if the particle scatters more light toward the forward direction, is negative if more light is scattered toward the

backscattering direction, and vanishes if the scattering is symmetric with respect to the plane perpendicular to the incidence direction.

An important difference between the regular and normalized matrices is that the latter do not possess the property of additivity. Consider, for example, a small volume element containing N_1 particles of type 1 and N_2 particles of type 2. The total scattering matrix of the volume element is obtained by adding the scattering matrices of all particles,

$$\mathbf{F} = N_1\langle \mathbf{F}_1 \rangle + N_2\langle \mathbf{F}_2 \rangle\,, \tag{110}$$

whereas the respective normalized matrix is given by

$$\widetilde{\mathbf{F}} = \frac{N_1\langle C_{\rm sca1}\rangle\widetilde{\mathbf{F}}_1 + N_2\langle C_{\rm sca2}\rangle\widetilde{\mathbf{F}}_2}{N_1\langle C_{\rm sca1}\rangle + N_2\langle C_{\rm sca2}\rangle}. \tag{111}$$

The traditional way of specifying the elements of the normalized scattering matrix is to tabulate their numerical values at a representative grid of scattering angles. A more mathematically appealing and efficient approach is to expand the scattering matrix elements in so-called generalized spherical functions $P^s_{mn}(\cos\Theta)$ or Wigner functions $d^s_{mn}(\Theta) = \mathrm{i}^{n-m}P^s_{mn}(\cos\Theta)$ (de Haan et al. 1987):

$$a_1(\Theta) = \sum_{s=0}^{s_{\rm max}} \alpha^s_1 P^s_{00}(\cos\Theta) = \sum_{s=0}^{s_{\rm max}} \alpha^s_1 d^s_{00}(\Theta), \tag{112}$$

$$a_2(\Theta) + a_3(\Theta) = \sum_{s=2}^{s_{\rm max}} (\alpha^s_2 + \alpha^s_3) P^s_{22}(\cos\Theta) = \sum_{s=2}^{s_{\rm max}} (\alpha^s_2 + \alpha^s_3) d^s_{22}(\Theta), \tag{113}$$

$$a_2(\Theta) - a_3(\Theta) = \sum_{s=2}^{s_{\rm max}} (\alpha^s_2 - \alpha^s_3) P^s_{2,-2}(\cos\Theta) = \sum_{s=2}^{s_{\rm max}} (\alpha^s_2 - \alpha^s_3) d^s_{2,-2}(\Theta), \tag{114}$$

$$a_4(\Theta) = \sum_{s=0}^{s_{\rm max}} \alpha^s_4 P^s_{00}(\cos\Theta) = \sum_{s=0}^{s_{\rm max}} \alpha^s_4 d^s_{00}(\Theta), \tag{115}$$

$$b_1(\Theta) = \sum_{s=2}^{s_{\rm max}} \beta^s_1 P^s_{02}(\cos\Theta) = -\sum_{s=2}^{s_{\rm max}} \beta^s_1 d^s_{02}(\Theta), \tag{116}$$

$$b_2(\Theta) = \sum_{s=2}^{s_{\rm max}} \beta^s_2 P^s_{02}(\cos\Theta) = -\sum_{s=2}^{s_{\rm max}} \beta^s_2 d^s_{02}(\Theta). \tag{117}$$

The number of nonzero terms in these expansions is in principle infinite. In practice the expansions are truncated at $s = s_{\rm max}$ with $s_{\rm max}$ chosen such that the corresponding finite sums differ from the respective scattering matrix elements on the entire interval $\Theta \in [0, \pi]$ within the desired numerical accuracy.

The properties of the generalized spherical functions and the Wigner d functions are well known (e.g., Hovenier and van der Mee 1983; Mishchenko et

al. 2002). For given m and n, either type of functions with $s \geq \max(|m|, |n|)$ forms a complete orthonormal set of functions of $\cos\Theta \in [-1, +1]$. Using the corresponding orthogonality relation, we obtain from (112)–(117)

$$\alpha_1^s = \left(s + \frac{1}{2}\right) \int_0^\pi \mathrm{d}\Theta \sin\Theta a_1(\Theta) d_{00}^s(\Theta), \tag{118}$$

$$\alpha_2^s + \alpha_3^s = \left(s + \frac{1}{2}\right) \int_0^\pi \mathrm{d}\Theta \sin\Theta [a_2(\Theta) + a_3(\Theta)] d_{22}^s(\Theta), \tag{119}$$

$$\alpha_2^s - \alpha_3^s = \left(s + \frac{1}{2}\right) \int_0^\pi \mathrm{d}\Theta \sin\Theta [a_2(\Theta) - a_3(\Theta)] d_{2,-2}^s(\Theta), \tag{120}$$

$$\alpha_4^s = \left(s + \frac{1}{2}\right) \int_0^\pi \mathrm{d}\Theta \sin\Theta a_4(\Theta) d_{00}^s(\Theta), \tag{121}$$

$$\beta_1^s = -\left(s + \frac{1}{2}\right) \int_0^\pi \mathrm{d}\Theta \sin\Theta b_1(\Theta) d_{02}^s(\Theta), \tag{122}$$

$$\beta_2^s = -\left(s + \frac{1}{2}\right) \int_0^\pi \mathrm{d}\Theta \sin\Theta b_2(\Theta) d_{02}^s(\Theta). \tag{123}$$

These formulas suggest a simple, although not always the most elegant and efficient way to compute the expansion coefficients by evaluating the integrals numerically using a suitable quadrature formula (de Rooij and van der Stap 1984). This procedure assumes the knowledge of the scattering matrix elements at the quadrature division points.

Since the Wigner d functions possess convenient mathematical properties and can be efficiently computed by using a simple and numerically stable recurrence relation, expansions (112)–(117) offer several practical advantages. For example, if the expansion coefficients appearing in these expansions are known, then the elements of the normalized scattering matrix can be easily calculated for practically any number of scattering angles with a minimal expense of computer time. Hence instead of tabulating the elements of the scattering matrix for a large number of scattering angles and using interpolation in order to find the scattering matrix at intermediate points, one can provide a complete and accurate specification of the scattering matrix by tabulating a limited number of numerically significant expansion coefficients. Another advantage of expansions (112)–(117) is that the d functions obey an addition theorem and thereby provide an elegant analytical way of calculating the coefficients in a Fourier decomposition of the normalized phase matrix in azimuth used to efficiently handle the azimuthal dependence of the solution of the vector radiative transfer equation (de Haan et al. 1987). One more advantage is that using the T-matrix method, the expansion coefficients can be calculated analytically without computing the scattering matrix itself (Mishchenko 1991).

The expansion coefficients obey the general inequalities $|\alpha_j^s| \leq 2s+1$ ($j = 1, 2, 3, 4$) and $|\beta_j^s| < 0.7(2s + 1)$ ($j = 1, 2$) (van der Mee and Hovenier 1990).

Since $d^s_{00}(\Theta)$ is also a Legendre polynomial $P_s(\cos\Theta)$, (112) is the well-known expansion of the phase function in Legendre polynomials (Chandrasekhar 1960). The identity $P_0(\cos\Theta) \equiv 1$ and (108) and (112) yield $\alpha^0_1 \equiv 1$, while the orthogonality property of the Wigner d functions and (109) result in the relation $\langle\cos\Theta\rangle = \alpha^1_1/3$.

6 Scale Invariance Rule

A fundamental property of electromagnetic scattering is the scale invariance rule, which states the following: If we multiply all particle dimensions by a constant factor f (thereby not changing the particle shape) and multiply the wave numbers k_1 and k_2 in the exterior and interior regions, respectively, by a factor $1/f$, then all dimensionless scattering and absorption characteristics of the particle do not change. This rule can be reformulated as follows: If the particle geometry is characterized by the shape and a typical dimension a (for example, the largest or the smallest particle dimension or the radius of the surface- or volume-equivalent sphere), then the dimensionless scattering characteristics do not depend on specific values of a, k_1, and k_2, but rather depend on the product of a and k_1, traditionally called the size parameter x, and the ratio of k_2 to k_1 which is simply the relative refractive index $\mathrm{m} = \mathrm{k}_2/\mathrm{k}_1 = \mathrm{m}_2/\mathrm{m}_1$. [The size parameter can also be expressed in terms of the wavelength of the incident wave in the exterior region $\lambda = 2\pi/\mathrm{k}_1$ as $x = 2\pi a/\lambda_1$]. The scale invariance rule is obeyed by the products of k_1^2 and the elements of the phase and scattering matrices; the products of k_1^2 and the optical cross sections; the products of k_1^2 and the extinction matrix elements; the efficiency factors; the elements of the normalized scattering matrix; the coefficients in (112)–(117); the single-scattering albedo; and the asymmetry parameter. The scale invariance rule can be very helpful in practice because it makes a single computation or measurement applicable to all couples (size, wavelength) with the same ratio size/wavelength, provided that the relative refractive index does not change. This rule underlies the basic idea of the microwave analog technique for laboratory measurements of electromagnetic scattering by small particles (Section 9).

7 Exact Theoretical Techniques

The scattering characteristics introduced in previous sections are intimately related to physical and geometrical parameters of particles such as size, shape, refractive index, and orientation. Therefore, understanding various optical phenomena and developing particle characterization techniques require accurate quantitative knowledge of the electromagnetic scattering interaction as a function of the particle parameters. Although all needs of a practitioner interested in light scattering by spherical particles may be well served by

the Lorenz-Mie theory, scattering properties of nonspherical particles must be either computed using a sophisticated theory or measured experimentally. Both approaches have their strengths, weaknesses, and limitations, and only a combination of various theoretical and experimental approaches can lead to significant advances in characterizing electromagnetic scattering by nonspherical particles.

Most of the exact theoretical techniques belong to one of two broad categories. Differential equation methods compute the scattered field by solving the Maxwell or the vector wave equations in the frequency or in the time domain, whereas integral equation methods are based on the volume or surface integral counterparts of the Maxwell equations. This section briefly reviews several widely used exact theoretical approaches. More detailed information can be found in the recent book edited by Mishchenko et al. (2000a).

The separation of variables method (SVM) for spheroids was developed by Oguchi (1973) and Asano and Yamamoto (1975). SVM solves the scattering problem in the spheroidal coordinate system by means of expanding the incident, internal, and scattered fields in vector spheroidal wave functions. The expansion coefficients of the incident field are computed analytically, whereas the unknown expansion coefficients of the internal and scattered fields are determined by applying the boundary conditions (10). Because the vector spheroidal wave functions are not orthogonal on the spheroid surface, this procedure yields an infinite set of linear algebraic equations for the unknown coefficients which must be truncated and solved numerically. SVM was significantly improved by Voshchinnikov and Farafonov (1993) and Kurtz and Salib (1993). Numerical factors have limited the applicability of SVM to semi-major-axis size parameters less than about 40. The obvious limitation of the technique is that it applies only to spheroidal scatterers, whereas the main advantage is that it produces very accurate results and is applicable to spheroids with extreme aspect ratios. SVM was extended to core-mantle spheroids by Onaka (1980), Cooray and Ciric (1992), and Farafonov et al. (1996). Further references can be found in the review by Ciric and Cooray (2000) and the book by Li et al. (2002).

The finite element method (FEM) is a differential equation technique that computes the scattered field by solving numerically the vector Helmholtz equation subject to the standard boundary conditions (Silvester and Ferrari 1996). The particle is imbedded in a finite computational domain discretized into many cells with about 10 to 20 cells per wavelength. The electric field values are specified at the nodes of the cells and are initially unknown. Using the boundary conditions, the differential equation is converted into a matrix equation for the unknown node field values. The latter is solved using the standard Gaussian elimination or preconditioned iterative techniques such as the conjugate gradient method. Although scattering in the far-field zone is an open-space problem, FEM is always implemented in a finite computational domain in order to limit the number of unknowns. Therefore, approximate

absorbing boundary conditions must be imposed at the outer boundary of the computational domain in order to suppress wave reflections back into the domain and permit the numerical analogs of the outward-propagating wave to exit the domain almost as if it were infinite. Another way of enforcing the radiation condition is the so-called unimoment method (Morgan 1980). FEM can be applied to arbitrarily shaped and inhomogeneous particles and is simple in concept and implementation. However, FEM computations are spread over the entire computational domain rather than confined to the scatterer itself, thereby making the technique slow and limited to size parameters less than about 10. The finite spatial discretization and the approximate absorbing boundary condition limit the accuracy of the method. Further information about FEM can be found in Silvester and Ferrari (1996), Volakis et al. (1998), and Jin (2002).

Unlike FEM, the finite difference time domain method (FDTDM) calculates electromagnetic scattering in the time domain by directly solving Maxwell's time-dependent curl equations (2) and (4) (Yee 1966). The space and time derivatives of the electric and magnetic fields are approximated using a finite difference scheme with space and time discretizations selected so that they constrain computational errors and ensure numerical stability of the algorithm. Since the scattering object is imbedded in a finite computational domain, absorbing boundary conditions are employed to model scattering in the open space (Berenger 1996). Modeling scattering objects with curved boundaries using rectangular grid cells causes a staircasing effect and increases numerical errors, especially for particles with large relative refractive indices. This effect is reduced using special techniques (Yang and Liou 2000; Sun and Fu 2000). Since FDTDM computes the near field in the time domain, a special near zone to far zone transformation must be invoked in order to compute the scattered far field in the frequency domain (Yang and Liou 1996; Taflove and Hagness 2000). FDTDM shares the advantages of FEM as well as its limitations in terms of accuracy and size parameter range. Additional information on FDTDM and its applications can be found in the book by Kunz and Luebbers (1993) and in the review by Yang and Liou (2000).

The point matching method (PMM) is a differential equation technique based on expanding the incident and internal fields in vector spherical wave functions (VSWFs) regular at the origin and expanding the scattered field outside the scatterer in outgoing VSWFs. The expansion coefficients of the incident field are computed analytically, whereas the coefficients of the internal and scattered fields are found by truncating the expansions to a finite size and matching the fields at the surface of the scatterer via the application of the boundary conditions. In the simple PMM, the fields are matched at as many points on the surface as there exist unknown expansion coefficients (Oguchi 1973). The simple PMM often produces poorly converging and unstable results, which may be attributed to the fact that it relies on

the Rayleigh hypothesis. The convergence problem of the simple PMM appears to be partly ameliorated in the generalized PMM (GPMM) by creating an overdetermined system of equations for the unknown coefficients by means of matching the fields in the least squares sense at a number of surface points significantly greater than the number of unknowns (Morrison and Cross 1974). The performance of GPMM is further improved by employing multiple spherical expansions to describe the fields both inside and outside the scattering object (Joo and Iskander 1990; Al-Rizzo and Tranquilla 1995). This multiple-expansion GPMM (ME-GPMM) does not rely on the Rayleigh hypothesis and is otherwise known as the generalized multipole technique, discrete sources method, and Yasuura method (Wriedt 1999; Doicu et al. 2000).

The interaction of a plane electromagnetic wave with an object of volume V_{INT} is fully described by the volume integral equation (28). The calculation of the scattered field using (28) would be straightforward except that the internal electric field is unknown. Therefore, this equation must first be solved for the internal field. The integral in (28) is approximated by discretizing the interior region into N cubic cells of a volume ΔV with about 10 to 20 cells per wavelength and assuming that the electric field and the refractive index within each cell are constant:

$$\mathbf{E}(\mathbf{r}_i) = \mathbf{E}^{\mathrm{inc}}(\mathbf{r}_i) + \mathrm{k}_1^2 \Delta V \sum_{j=1}^{N} \overleftrightarrow{G}(\mathbf{r}_i, \mathbf{r}_j) \cdot \mathbf{E}(\mathbf{r}_j)[\mathrm{m}^2(\mathbf{r}_j) - 1], \quad i = 1, ..., N, \tag{124}$$

where $\mathbf{r}_i \in V_{\mathrm{INT}}$ is the central point of the ith cell. Equations (124) form a system of N linear algebraic equations for the N unknown internal fields $\mathbf{E}(\mathbf{r}_i)$ and are solved numerically. Once the internal fields are found, the external field is determined from

$$\mathbf{E}(\mathbf{r}) = \mathbf{E}^{\mathrm{inc}}(\mathbf{r}) + \mathrm{k}_1^2 \Delta V \sum_{j=1}^{N} \overleftrightarrow{G}(\mathbf{r}, \mathbf{r}_j) \cdot \mathbf{E}(\mathbf{r}_j)[\mathrm{m}^2(\mathbf{r}_j) - 1], \quad \mathbf{r} \in V_{\mathrm{EXT}}. \tag{125}$$

Finally, the scattered field is computed by subtracting the incident field from the external field. This version of the volume integral equation method (VIEM) is known as the method of moments (MOM). Since the free space dyadic Green's function becomes singular as $|\mathbf{r} - \mathbf{r}'| \to 0$, special techniques must be used to handle the self-interaction term ($j = i$) in the sum on the right-hand side of (124) (Lakhtakia and Mulholland 1993). The straightforward approach to solving the MOM matrix equation using the standard Gaussian elimination is not practical for size parameters exceeding unity. The conjugate gradient method together with the fast Fourier transform (Peterson et al. 1998) can be applied to significantly larger size parameters and significantly reduces computer memory requirements. The standard drawback of using a preconditioned iterative technique is that computations must be fully repeated for each new illumination direction.

Another version of VIEM is the so-called discrete dipole approximation (DDA). Whereas MOM deals with the *actual* electric fields in the central points of the cells, DDA exploits the concept of *exciting* fields. DDA is based on partitioning the particle into a number N of elementary polarizable units called dipoles. The electromagnetic response of the dipoles to the local electric field is assumed to be known. The field exciting a dipole is a superposition of the external field and the fields scattered by all other dipoles. This allows one to write a system of N linear equations for N fields exciting the N dipoles. The numerical solution of the DDA matrix equation is then used to compute the N partial fields scattered by the dipoles and thus the total scattered field. Although the original derivation of the DDA by Purcell and Pennypacker (1973) was heuristic, Lakhtakia and Mulholland (1993) showed that DDA can be derived from (28) and is closely related to MOM.

The major advantages of MOM and DDA are that they automatically satisfy the radiation condition at infinity (31), are confined to the scatterer itself, thereby resulting in fewer unknowns than the differential equation methods, and can be applied to inhomogeneous, anisotropic, and optically active scatterers. However, the numerical accuracy of the methods is relatively low and improves only slowly with increasing N, whereas the computer time grows rapidly with increasing size parameter (Draine and Flatau 1994; Evans and Stephens 1995; Okamoto et al. 1995). Another disadvantage of the techniques is the need to repeat the entire calculation for each new direction of incidence. Further information on MOM and DDA and their applications can be found in Miller et al. (1991) and Draine (2000).

Equation (28) is a Fredholm-type integral equation with a singular kernel at $\mathbf{r}' = \mathbf{r}$. Holt et al. (1978) removed the singularity by applying the Fourier transform to the internal field and converting the volume integral into an integral in the wave number coordinate space. Discretization of the latter integral results in a matrix equation which is solved numerically and gives the scattered field. A limitation of this Fredholm integral equation method (FIEM) is that the matrix elements must be evaluated analytically, thereby requiring different programs for each shape and restricting computations to only a few models such as spheroids, triaxial ellipsoids, and finite circular cylinders. The majority of reported FIEM computations pertain to size parameters smaller than 5 and tend to be rather time consuming (Holt 1982).

The Lorenz-Mie theory can be extended to clusters of spheres by using the translation addition theorem for vector spherical wave functions (Bruning and Lo 1971; Borghese et al. 1979; Fuller 1991). The total field scattered by a multi-sphere cluster can be expressed as a superposition of individual fields scattered from each sphere. The external electric field illuminating the cluster and the individual fields scattered by the component spheres are expanded in VSWFs with origins at the individual sphere centers. The orthogonality of the VSWFs in the sphere boundary conditions is exploited by applying the translation addition theorem in which a VSWF centered at one sphere

origin is re-expanded about another sphere origin. This procedure ultimately results in a matrix equation for the scattered-field expansion coefficients of each sphere. Numerical solution of this equation for the specific incident wave gives the individual scattered fields and thereby the total scattered field. Alternatively, inversion of the cluster matrix equation gives sphere-centered transition matrices that transform the expansion coefficients of the incident wave into the expansion coefficients of the individual scattered fields. In the far-field region, the individual scattered-field expansions can be transformed into a single expansion centered at a single origin inside the cluster. This procedure gives the T matrix that transforms the incident-wave expansion coefficients into the single-origin expansion coefficients of the total scattered field (Mackowski 1994) and can be used in the analytical averaging of scattering characteristics over cluster orientations (Fucile et al. 1993; Mackowski and Mishchenko 1996). The superposition method (SM) has been extended to spheres with one or more eccentrically positioned spherical inclusions (Borghese et al. 1994; Fuller 1995; Videen et al. 1995) and to clusters of dielectric spheroids in an arbitrary configuration (Ciric and Cooray 2000). Because of the analyticity of its mathematical formulation, SM is capable of producing very accurate results. Fuller and Mackowski (2000) gave a detailed review of SM for compounded spheres.

The T-matrix method (TMM) is based on expanding the incident field in VSWFs regular at the origin and expanding the scattered field outside a circumscribing sphere of the scatterer in VSWFs regular at infinity. The T matrix transforms the expansion coefficients of the incident field into those of the scattered field and, if known, can be used to compute any scattering characteristic of the particle. TMM was initially developed by Waterman (1971) for single homogeneous objects and was generalized to multilayered scatterers and arbitrary clusters of nonspherical particles by Peterson and Ström (1973, 1974). For spheres, all TMM formulas reduce to those of the Lorenz-Mie theory. In the case of clusters composed of spherical components, the T-matrix method reduces to the multi-sphere SM (Mackowski 1994).

The T matrix for single homogeneous and multilayered scatterers is usually computed using the extended boundary condition method (EBCM; Waterman 1971), which explicitly avoids the use of the Rayleigh hypothesis. EBCM can be applied to any particle shape, although computations become much simpler and more efficient for bodies of revolution. Special procedures were developed to improve the numerical stability of EBCM computations for large size parameters and/or extreme aspect ratios (Mishchenko and Travis 1998). Recent work has demonstrated the practical applicability of EBCM to particles without axial symmetry, e.g., ellipsoids, cubes, and finite polyhedral cylinders (e.g., Laitinen and Lumme 1998; Doicu et al. 2000; Kahnert et al. 2001; Havemann and Baran 2001). The computation of the T matrix for a cluster assumes that the T matrices of all components are known and is based on the use of the translation addition theorem for VSWFs (Pe-

terson and Ström 1973). The loss of efficiency for particles with large aspect ratios or with shapes lacking axial symmetry is the main drawback of TMM. The main advantages of TMM are high accuracy, speed, and applicability to particles with equivalent-sphere size parameters exceeding 180 (Mishchenko and Macke 1999). Mishchenko (1991), Khlebtsov (1992), and Mackowski and Mishchenko (1996) developed analytical orientation averaging procedures which make TMM computations for randomly oriented particles as fast as those for a particle in a fixed orientation. Further information can be found in Mishchenko et al. (2002).

The only methods yielding very accurate results for particles comparable to and larger than a wavelength are SVM, TMM, and SM. SVM, TMM, SM, and ME-GPMM have been used in computations for particles significantly larger than a wavelength. The first three techniques appear to be the most efficient in application to bodies of revolution. The analytical orientation averaging procedure makes TMM the most efficient technique for randomly oriented particles with moderate aspect ratios. Particles with larger aspect ratios can be treated with SVM, an iterative EBCM, and ME-GPMM. Computations for anisotropic objects and homogeneous and inhomogeneous particles lacking rotational symmetry often have to rely on more flexible techniques such as FEM, FDTDM, MOM, and DDA. These techniques are simple in concept and computer implementation and have comparable performance characteristics, although their simplicity and flexibility are often accompanied by lower efficiency and accuracy and by stronger practical limitations on the maximal size parameter. A number of software implementations of the techniques described in this section are currently available on-line and many of them are in the public domain (Flatau 2000; Wriedt 2000).

8 Approximations

Any approximate theory of light scattering is based on a simplifying assumption that substantially limit its range of applicability. For example, Rayleigh (1897) derived an approximation for scattering in the small-particle limit ($x \ll 1$) by assuming that the incident field inside and near the particle behaves almost as an electrostatic field and the internal field is homogeneous. The conditions of validity of the Rayleigh-Gans approximation (RGA) (otherwise known as the Rayleigh-Debye or Born approximation) are $x|\mathrm{m}-1| \ll 1$ and $|\mathrm{m}-1| \ll 1$. Hence particles are assumed to be not too large (although they may be larger than in the case of Rayleigh scattering) and optically "soft." The fundamental RGA assumption is that each small-volume element of the scattering object is excited only by the incident field. The scattered field is then computed from (30) after substituting $\mathbf{E}(\mathbf{r}') = \mathbf{E}^{\mathrm{inc}}(\mathbf{r}')$. The anomalous diffraction approximation (ADA) was introduced by van de Hulst (1957) as a means of computing the extinction cross section for large, optically soft spheres with $x \gg 1$ and $|\mathrm{m}-1| \ll 1$. Since the second condition

means that rays are weakly deviated as they cross the particle boundary and are negligibly reflected, ADA assumes that extinction is caused by absorption of light passing through the particle and by the interference of light passing through and around the particle.

The practical importance of approximate theories diminishes as various exact techniques mature and become applicable to a wider range of problems, while computers become ever more powerful. However, approximate theories still remain a valuable source of physical insight into the process of scattering and absorption by nonspherical particles (Baran et al. 1998; Jones 1999; Kokhanovsky 2001). Furthermore, it is likely that at least one approximation, the geometrical optics method, will never become obsolete because its accuracy only improves as the particle size parameter grows, whereas all exact theoretical techniques for nonspherical particles cease to be practical when the size parameter exceeds a certain threshold.

The geometrical optics approximation (GOA) (otherwise known as the ray-tracing or ray optics approximation) is a universal method for computing electromagnetic scattering by arbitrarily shaped particles with sizes much larger than the wavelength of the incident light. GOA assumes that the incident plane wave can be represented as a collection of independent parallel rays. The history of each ray impinging on the particle surface is traced using Snell's law and Fresnel's formulas. Each incident ray is partially reflected and partially refracted into the particle. The refracted ray may emerge after another refraction, possibly after one or more internal reflections, and may be attenuated by absorption inside the particle. Each internal ray is traced until its intensity decreases below a predefined cutoff value. Varying the polarization state of the incident rays, sampling all escaping rays into predefined narrow angular bins, and adding incoherently the respective Stokes parameters yields a quantitative representation of the particle scattering properties in terms of the ray-tracing phase matrix $\mathbf{Z}^{\mathrm{RT}}$. Because all rays impinging on the particle surface are either scattered or absorbed irrespective of their polarization state, the ray-tracing extinction matrix is always diagonal and is given by $\mathbf{K}^{\mathrm{RT}} = C_{\mathrm{ext}}^{\mathrm{RT}}\mathbf{\Delta}$. The ray-tracing extinction cross section $C_{\mathrm{ext}}^{\mathrm{RT}}$ does not depend on the polarization state of the incident light and is equal to the geometrical area G of the particle projection on the plane perpendicular to the incidence direction. Since the presence of the particle modifies the incident plane wave front by eliminating a part that has the shape and size of the geometrical projection of the particle, the ray-tracing scattering pattern must be supplemented by the computation of Fraunhofer diffraction of the incident wave on the particle projection. The diffraction component of the phase matrix $\mathbf{Z}^{\mathrm{D}}$ is confined to a narrow angular cone centered at the exact forward-scattering direction and is usually computed in the Kirchhoff approximation (Jackson 1998), thereby contributing only to the diagonal elements of the total phase matrix. The diffraction component $\mathbf{K}^{\mathrm{D}}$ of the total extinction matrix is equal to $\mathbf{K}^{\mathrm{RT}}$. We thus have

$\mathbf{Z}^{\rm GO} = \mathbf{Z}^{\rm RT} + \mathbf{Z}^{\rm D} = \mathbf{Z}^{\rm RT} + Z_{11}^{\rm D}\mathbf{\Delta}$, $\mathbf{K}^{\rm GO} = \mathbf{K}^{\rm RT} + \mathbf{K}^{\rm D} = C_{\rm ext}^{\rm GO}\mathbf{\Delta}$, where $C_{\rm ext}^{\rm GO} = C_{\rm ext}^{\rm RT} + C_{\rm ext}^{\rm D} = 2G$. The total scattering cross section is the sum of the ray-tracing and diffraction components: $C_{\rm sca}^{\rm GO} = C_{\rm sca}^{\rm RT} + C_{\rm sca}^{\rm D}$. Since the diffracted energy is not absorbed, the diffraction scattering cross section is equal to the diffraction extinction cross section: $C_{\rm sca}^{\rm D} = C_{\rm ext}^{\rm D} = G$. The ray-tracing scattering cross section $C_{\rm sca}^{\rm RT}$ is found from $\mathbf{Z}^{\rm RT}$ and (76).

The main advantage of GOA is that it can be applied to essentially any shape. However, this technique is approximate by definition, and its range of applicability in terms of the smallest size parameter must be checked by comparing GOA results with exact numerical solutions of the Maxwell equations. It appears that although the main geometrical optics features can be qualitatively reproduced by particles with size parameters less than 100, obtaining good quantitative accuracy in GOA computations of the phase matrix still requires size parameters exceeding a few hundred (Wielaard et al. 1997). Even then GOA fails to reproduce scattering features caused by interference and diffraction effects (Hansen and Travis 1974; Mishchenko and Macke 1998). To improve GOA, Ravey and Mazeron (1982) (see also Muinonen 1989; Liou et al. 2000) developed the so-called physical optics or Kirchhoff approximation (KA). This approach is based on expressing the scattered field in terms of the electric and magnetic fields on the exterior side of the particle surface. The latter are computed approximately using Fresnel formulas and the standard ray-tracing procedure. KA partially preserves the phase information and reproduces some physical optics effects completely ignored by the standard GOA.

9 Measurement Techniques

Existing measurement techniques fall into two categories: (i) scattering of visible or infrared light by particles with sizes from several hundredths of a micron to several hundred microns; and (ii) microwave scattering by millimeter- and centimeter-sized objects. Measurements in the visible and infrared benefit from the availability of sensitive detectors (photomultipliers and avalanche semiconductor photodiodes), intense sources of radiation (lasers), and high-quality optical elements. They involve cheaper and more portable instrumentation and can be performed in the field as well as in the laboratory. By contrast, microwave scattering experiments require more cumbersome and expensive instrumentation and large measurement facilities.

Many detectors of electromagnetic energy are polarization-insensitive: the detector response is determined only by the first Stokes parameter of the beam impinging on the detector. Therefore, in order to measure all elements of the scattering matrix one must use various optical elements that can vary the polarization state of light before and after scattering in a controllable way. In Fig. 5 (adapted from Hovenier 2000), the beam produced by a laser passes through a linear polarizer and a polarization modulator and then illuminates

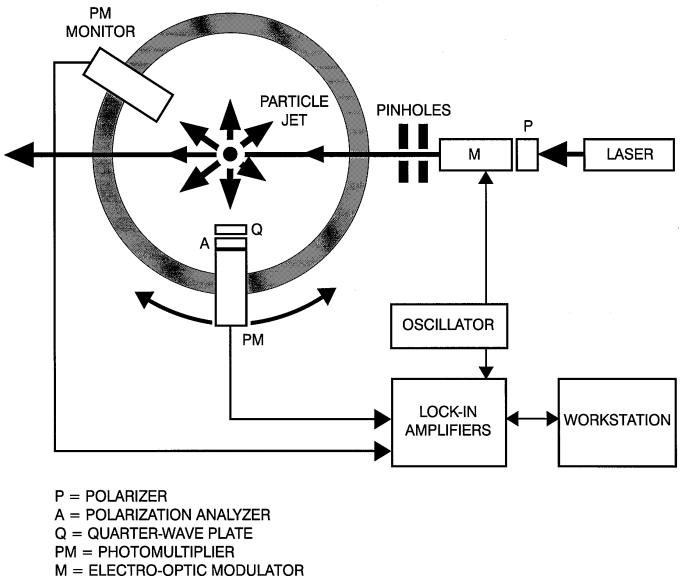

Fig. 5. Scheme of an experimental setup employing visible light.

particles contained in the scattering chamber. Light scattered by the particles at an angle Θ passes a quarter-wave plate and a polarization analyzer, after which its intensity is measured by a detector. The Stokes vector of the beam reaching the detector, $\mathbf{I}'$, is given by $\mathbf{I}' \propto \mathbf{AQF}(\Theta)\mathbf{MPI} = \mathbf{AQ}N\langle\mathbf{F}(\Theta)\rangle\mathbf{MPI}$, where $\mathbf{I}$ is the Stokes vector of the beam leaving the light source, $\mathbf{A}, \mathbf{Q}, \mathbf{M}$ and $\mathbf{P}$ are 4×4 Mueller transformation matrices of the analyzer, quarter-wave plate, modulator, and polarizer, respectively, $\mathbf{F}(\Theta)$ is the total scattering matrix of the particles contributing to the scattered beam, N is the number of the particles, and $\langle\mathbf{F}(\Theta)\rangle$ is the ensemble-averaged scattering matrix per particle. It is assumed that the scattering plane serves as the reference frame for defining the Stokes parameters. The Mueller matrices of the polarizer, modulator, quarter-wave plate, and analyzer depend on their orientation with respect to the scattering plane and can be precisely varied. Because the detector measures only the first element of the Stokes vector $\mathbf{I}'$, several measurements with different orientations of the optical components with respect to the scattering plane are required for the full determination of the scattering matrix. This procedure is repeated at different scattering angles in order to determine the angular profile of the scattering matrix.

Early measurements of the scattering matrix used a simple subtraction method which relied on pairs of intensities measured separately with different combinations of polarizing elements; the results were subtracted in order to obtain the scattering matrix elements. This technique has low accuracy because of the need to determine small differences between two large signals.

The measurements of the two large signals are separated in time and imply that the sensitivity of the detector and the scattering sample (e.g., the number N of scattering particles) do not change with time, which is often not the case. Hunt and Huffman (1973) developed the technique of a high-frequency sinusoidal modulation in time of the polarization of light before scattering (Fig. 5) combined with intensity normalization. Followed by lock-in detection, this technique increases the experimental accuracy by enabling direct measurements of the scattering matrix elements normalized by the (1, 1) element and yields the capability to determine several elements from only one detected signal.

Measurements at visible and infrared wavelengths often suffer from the lack of accurate independent characterization of particle size and morphology, which makes it difficult to compare experimental and theoretical results. The number of particles N contributing to the scattered beam is also seldom known, which precludes the absolute measurement of the (1, 1) element of the ensemble-averaged scattering matrix per particle $\langle \mathbf{F}(\Theta) \rangle$ [measurements of the elements other than the (1, 1) element are usually reported in the form of N-independent ratios of the elements to the (1, 1) element]. Another drawback is that the arrangement of the source of light and the detector usually precludes measurements at scattering angles close to 0° and 180°. This makes problematic the absolute measurement of the phase function by means of satisfying the normalization condition (108). In consequence, experimental phase functions are often normalized to the value at a fixed scattering angle.

The error of deriving the scattering cross section per particle by integrating the scattered intensity over all scattering angles also relies on the knowledge of N and depends on how much of the forward- and back-scattered energy is not detected (Anderson et al. 1996). The phase function of particles larger than the wavelength has a strong and narrow diffraction peak that may contain more than 50% of the total scattered energy. This factor alone can cause errors in the measured scattering cross section exceeding 50%. The extinction cross section is often determined by measuring the attenuation of directly transmitted beam. Specifically, the extinction cross section is proportional to the difference of the readings of detector 1 in Fig. 3 corresponding to the situations without and with the particles interposed between the source of light and the detector (Section 3). This measurement unavoidably suffers from the problem that a detector with a finite aperture picks up some of the light *scattered* by the particles in the forward direction. Depending on the average particle size and thus the magnitude and angular width of the diffraction component of the phase function, the extinction can be underestimated by as much as a factor of 2. With potentially significant errors in the extinction and scattering cross sections, little may be said about the difference of the former and the latter, i.e., the absorption cross section, and the ratio of the latter to the former, i.e., the single-scattering albedo.

An instrument specifically designed for measurements at the exact backscattering direction is a lidar composed of a laser emitting a powerful beam and a receiving telescope-detector combination affixed to the laser (Sassen 2000; also the chapter by Gobbi). The laser beam is usually polarized either linearly ($P = 1, V = 0$) or circularly ($P = 1, V = \pm I$). The laser light scattered by aerosol and cloud particles is collected by the telescope, and its intensity and polarization characteristics are precisely measured. Since lidars measure backscattering from particles located at large distances from the instrument, the scattering angle can be made arbitrarily close to 180°. Important quantities measured by a polarization lidar are so-called linear and circular depolarization ratios. Because both ratios vanish for spherically symmetric scatterers, finite measured ratios may directly indicate the presence of nonspherical particles.

Measurements of scattering properties of millimeter- and centimeter-sized objects at microwave frequencies are important for such applications as remote sensing of precipitation and communication technology (Aydin 2000; Haferman 2000). In addition, the scale invariance rule (Section 6) states that particle size in the theoretical formulation of electromagnetic scattering is only encountered as a ratio to the wavelength. Therefore, the main idea of the microwave analog technique is to manufacture a centimeter-sized scattering object with desired shape and refractive index, measure the scattering of a microwave beam by this object, and finally extrapolate the result to other wavelengths (e.g., visible or infrared) by keeping the ratio size/wavelength fixed (Gustafson 2000).

In a modern microwave scattering setup, radiation from a transmitting conical horn antenna passes through a collimating lens and a polarizer. The lens produces a nearly flat wave front which is scattered by an analog particle model target. The scattered wave passes through another polarizer and lens and is measured by a receiving horn antenna. The receiver end of the setup can be positioned at any scattering angle from 0° to $\Theta_{\max} \cong 170°$, thereby providing measurements of the angular distribution of the scattered radiation. By varying the orientations of the two polarizers, one can measure all elements of the scattering matrix. Microwave measurements allow a much greater degree of control over the target size, shape, and orientation than optical/infrared measurements. Therefore, the results of controlled laboratory measurements at microwave frequencies can be easily compared with theory. Using special techniques, even the extinction cross section can be measured. Furthermore, it is possible to add the backscattering measurement capability ($\Theta = 180°$) by using the transmitting antenna as a receiver. A disadvantage of microwave measurements is that they can be performed only for one particle size, shape, and orientation at a time, thereby making ensemble averaging a time-consuming procedure. Various experimental aspects of the microwave analog technique were reviewed by Gustafson (2000).

A special class of instruments providing active polarization measurements for remote targets at microwave and radiowave frequencies are radars (Aydin 2000; Bringi and Chandrasekar 2001). Monostatic radars use the same antenna to transmit and receive electromagnetic waves and, therefore, are limited to measurements at the exact backscattering direction ($\Theta = 180°$). Bistatic lidars use one or more additional receiving antennas which provide supplementary information for other scattering angles.

10 Effects of Nonsphericity on Scattering Patterns

The most fundamental effects of particle nonsphericity on electromagnetic scattering are that the extinction matrix does not, in general, reduce to a direction- and polarization-independent scalar, the extinction, scattering, and absorption cross sections depend on the direction and polarization state of the incident beam, and the scattering matrix does not have the Lorenz-Mie structure given by (105). In general, all 16 elements of the scattering matrix can be nonzero and depend on the orientation of the scattering plane. Any of these effects can directly indicate the presence of nonspherical particles.

When nonspherical particles are randomly oriented and form a microscopically isotropic and mirror symmetric scattering medium (Section 5), the extinction matrix does degenerate to the scalar extinction cross section, and all optical cross sections become orientation- and polarization-independent. Moreover, the corresponding scattering matrix (89) possesses almost the same structure as the Lorenz-Mie scattering matrix. However, the remaining fundamental difference is that the (2, 2) element of the scattering matrix may differ from to the (1, 1) element and the (4, 4) element may differ from the (3, 3) element. This is demonstrated in Fig. 6, which depicts the elements of the normalized scattering matrix given by (106) for a narrow power law size distribution of spheres and surface-equivalent, randomly oriented oblate spheroids with an aspect ratio of 1.7 (Mishchenko et al. 1996b). The refractive index is 1.53 + 0.008i and the effective size parameter of the size distribution is 15. The computations were performed using the conventional Lorenz-Mie theory for spheres and the T-matrix method for spheroids (Mishchenko and Travis 1998).

Besides this qualitative difference which unequivocally distinguishes randomly oriented nonspherical particles from spheres, Fig. 6 also shows significant quantitative spherical-nonspherical differences. For example, the phase function for spheroids exhibits an enhanced side-scattering and a suppressed backscattering. The degree of linear polarization for unpolarized incident light $P_Q = -b_1/a_1$ for spheroids is positive at side-scattering angles and is negative for spheres. These conclusions are supported by systematic theoretical surveys of light scattering by ensembles of Chebyshev particles (Wiscombe and Mugnai 1988), spheroids (Mishchenko et al. 1996b), finite circular cylinders (Mishchenko et al. 1996a), and polycrystals (Takano and Liou 1995;

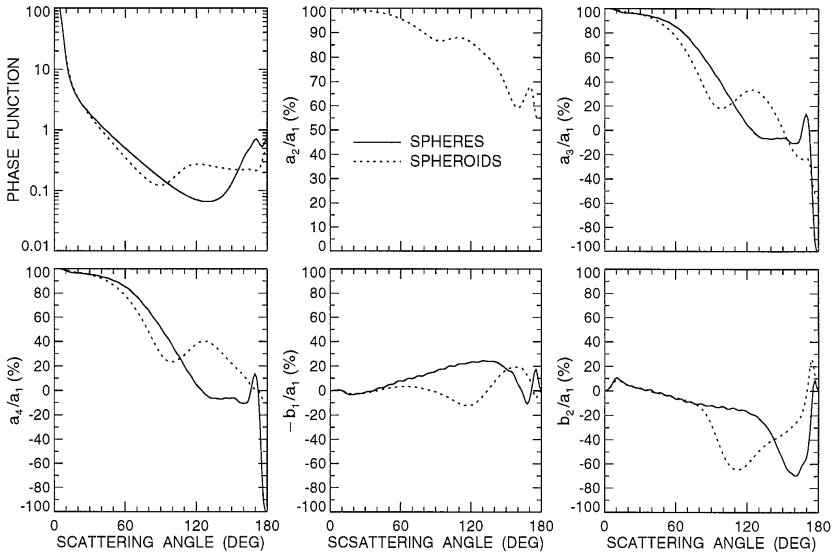

Fig. 6. Phase function and normalized scattering matrix elements for a power law size distribution of spheres and randomly oriented spheroids. The refractive index is 1.53 + 0.008i and the effective size parameter of the size distribution is 15.

Macke et al. 1996). Spherical-nonspherical differences in the elements of the scattering matrix are maximal for nonabsorbing particles and diminish with increasing absorption. Although differences in the optical cross sections, single scattering albedo, and asymmetry parameter can also be noticeable, they are usually much smaller than the differences in the elements of the scattering matrix. This does not apply, however, to particles with extreme aspect ratios (e.g., Zakharova and Mishchenko 2000, 2001).

Clusters of small monomers form a special class of nonspherical particles. Although scattering properties of randomly oriented two-sphere clusters closely resemble those of a single sphere (Mishchenko et al. 1995), the effect of cooperative phenomena in many-particle clusters can be very strong (Mackowski and Mishchenko 1996). Scattering properties of clusters are often a combination of those for a single monomer and those for a solid particle circumscribing the cluster and having the same average projected area (e.g., West 1991; Lumme 2000).

The ability to compute scattering by a specific shape does not necessarily mean the ability to theoretically reproduce scattering properties of real ensembles of nonspherical particles. More often than not, natural and artificial particle samples exhibit a great variety of shapes, thereby making questionable the potential of a single nonspherical shape to represent scattering properties of a particle ensemble. It can be demonstrated indeed that even after size and orientation averaging, essentially any particle shape

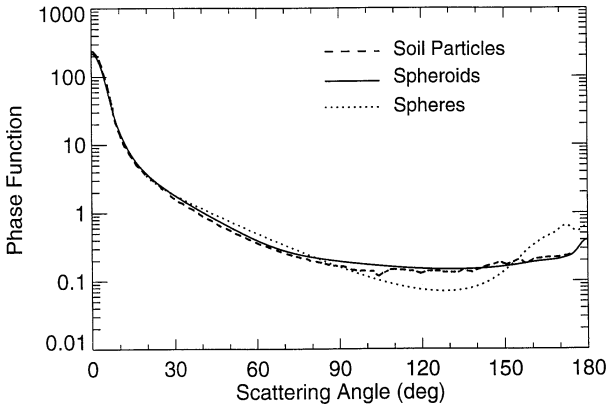

Fig. 7. Phase functions computed for a broad shape distribution of polydisperse spheroids and surface-equivalent spheres and measured by Jaggard et al. (1981) for natural wavelength-size soil particles.

produces a unique, shape-specific scattering pattern, whereas experimental measurements for real nonspherical particles usually show smooth, featureless patterns (e.g., Perry et al. 1978; Volten et al. 2001). Therefore, in theoretical computations, specific details of scattering patterns generated by various discrete shapes should be suppressed by averaging over a representative shape distribution. For example, the phase function shown in Fig. 7 by the solid curve was computed for a wide aspect-ratio distribution of micron-sized prolate and oblate spheroids with an index of refraction of 1.53 + 0.008i typical of dust-like aerosols at visible wavelengths. Unlike the phase function depicted by the dotted curve in Fig. 6 and calculated for spheroids with a fixed aspect ratio, the phase function for the shape distribution of spheroids is very smooth and featureless and, in fact, almost perfectly coincides with the phase function experimentally measured by Jaggard et al. (1981) for micron-sized irregularly shaped soil particles (Mishchenko et al. 1997).

This example may have two important ramifications. First, it suggests that the smooth scattering-angle dependence of the scattering matrix elements often observed for ensembles of natural and artificial nonspherical particles is caused by the diversity of particle shapes. Second, it may indicate that at least some scattering properties of irregular particles could be modeled using a shape mixture of simple particles such as spheroids. The assumption that particles chosen for the purposes of ensemble averaging need not be in one-to-one correspondence with the ensemble of irregular particles in hand and may have relatively simple shapes is central to the so-called statistical approach (Wiscombe and Mugnai 1988; Bohren and Singham 1991). The attractiveness of this approach is explained by the fact that it is often impossible to exactly specify the shapes and sizes of all particles forming a natural or artificial sample. Even if it were possible, the low efficiency of

the exact numerical scattering techniques applicable to arbitrarily shaped particles would require an enormous computational effort. The availability of techniques like the T-matrix method, which is very fast for randomly oriented rotationally symmetric particles and is applicable to large size parameters, makes the statistical approach quite practical (Hill et al. 1984; Mishchenko et al. 1997). Another plausible approach is to assume that scattering properties of an ensemble of irregular particles can be reproduced by mixing only a few statistically representative particle models created by a numerical random shape generator. This approach was pursued by Peltoniemi et al. (1989), Macke et al. (1996), and Muinonen (2000) by applying GOA to particles much larger than a wavelength and by Lumme (2000), who applied VIEM to particles with size parameters smaller than 6. Although this approach is more time-consuming and has a limited size parameter range, it may find more applications as computers become more powerful and methods like FEM, FDTDM, and VIEM become more efficient.

11 Remote Sensing and Radiation Balance Applications

Nonsphericity can significantly affect the results of remote sensing retrievals of mineral tropospheric aerosols. Indeed, large spherical-nonspherical phase function differences (Fig. 7) can result in an underestimation or an overestimation of the optical thickness if satellite reflectance measurements for dust-like tropospheric aerosols are analyzed using the Lorenz-Mie theory (Mishchenko et al. 1997; Kahn et al. 1997). The quantity directly entering the lidar equation is the so-called extinction-to-backscatter ratio $R_{\rm eb} = C_{\rm ext}/C_{\rm sca}a_1(\pi)$ (Reagan et al. 1989; Stephens 1994; also the chapter by Gobbi). The dashed curve in Fig. 8 (adapted from Mishchenko et al. 1997) demonstrates that spherical-nonspherical differences in $R_{\rm eb}$ can be very large and can cause lidar retrievals of the optical thickness for nonspherical aerosols based on the Lorenz-Mie theory to be unreliable. Nonsphericity can change not only the magnitude of the degree of linear polarization $P_Q(\Theta) = -b_1(\Theta)/a_1(\Theta)$, but even its sign (Mishchenko 1996b) thereby affecting polarimetric retrievals of dust-like tropospheric aerosols (Deuzé et al. 2000).

Despite the potentially strong effect of nonsphericity on aerosol remote sensing, the shape effect on the direct aerosol forcing of climate is rather weak. This means that if the optical thickness of nonspherical aerosols can be reliably determined, then the aerosol radiative forcing can be computed with high accuracy using the model of surface-equivalent spheres (Lacis and Mishchenko 1995). This result can be explained by small spherical-nonspherical differences in the aerosol single-scattering albedo and asymmetry parameter (Fig. 8). It is important to emphasize, however, that no cancellation of errors occurs if one consistently uses the Lorenz-Mie theory in retrieving the aerosol optical

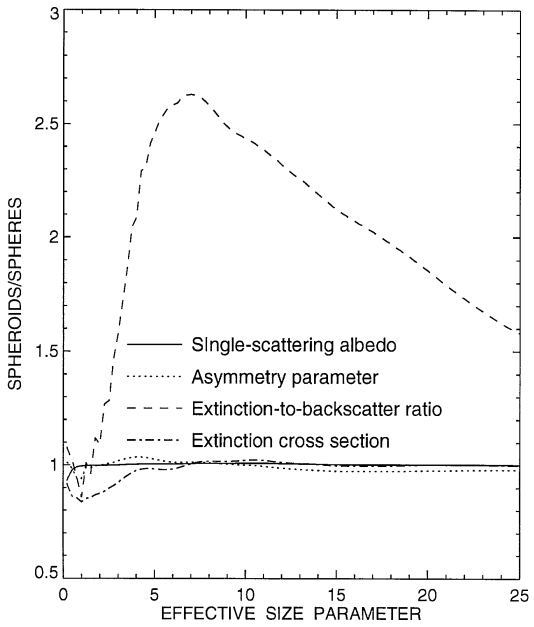

Fig. 8. Ratios of single-scattering characteristics of a shape mixture of polydisperse, randomly oriented spheroids to those of surface-equivalent spheres. The refractive index is 1.53+0.008i.

thickness and then in computing the aerosol radiative forcing for the retrieved optical thickness value.

Another radiatively important type of nonspherical particles in the atmosphere are cirrus ice crystals. In some cases, cirrus clouds exhibit remarkable optical phenomena such as halos, thereby indicating that ice crystals have regular shapes such as single or aggregated hexagonal columns and plates (Macke 1993; Takano and Liou 1995). However, for many cirrus clouds the halos are not seen even under suitable observation geometries and the ice particle phase function appears to be rather featureless (e.g., Francis 1995; Gayet et al. 1998). One way to model a featureless phase function is to assume that ice particles lack the perfect hexagonal structure and occur in a wide variety of shapes and to use the statistical approach outlined in the previous section. Another approach is to model scattering properties of a random ensemble of different shapes using a few randomly shaped particles and employing GOA (Macke et al. 1996; Muinonen 2000). Figure 9 compares phase functions computed at $\lambda = 0.65\,\mu\text{m}$ for the ISCCP water droplet model (Rossow and Schiffer 1999), regular hexagonal ice columns, and randomly shaped ice particles modeled as a randomized triadic Koch fractal (adapted from Mishchenko et al. 1996c). It is seen that the random-particle phase function is relatively featureless and does not show halos specific of

hexagonal crystals and pronounced rainbow and glory features exhibited by spherical water droplets. The differences in the phase functions depicted in Fig. 9 are even greater than those shown in Fig. 7 and produce much larger differences in the retrieved cirrus-cloud optical thickness (Mishchenko et al. 1996c).

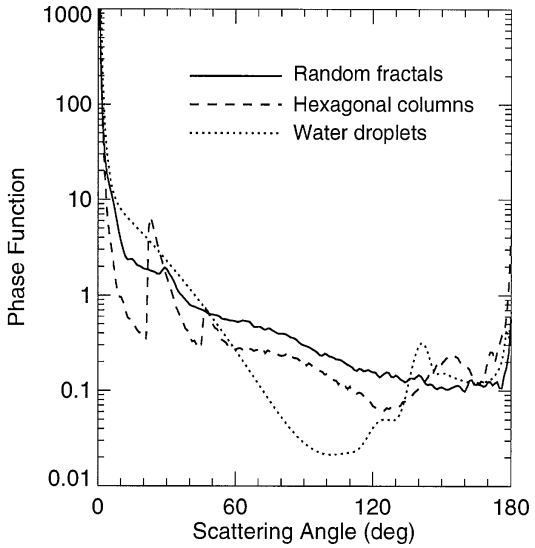

Fig. 9. Phase functions for the ISCCP water droplet model, hexagonal ice columns, and randomly shaped ice particles.

The effect of nonsphericity on the cirrus cloud radiative forcing can also be much stronger due to significantly larger spherical-nonspherical differences in the single-scattering characteristics. Figure 10 (adapted from Mishchenko et al. 1996c) shows that the global albedo of a liquid-water cloud at solar wavelengths can be significantly smaller than that of an optical-thickness equivalent ice cloud composed of hexagonal crystals and much smaller than that of an ice cloud composed of randomly shaped crystals. This result is explained by the fact that the asymmetry parameter for the randomly shaped crystals (0.752) is smaller than that for the hexagonal columns (0.816) and much smaller than that for the ISCCP water droplets (0.862) and emphasizes the importance of exact knowledge of the asymmetry parameter for real cirrus cloud particles. The potentially strong effect of nonsphericity on the cirrus cloud radiative forcing makes important accurate parameterizations of ice particle scattering properties. For example, the parameterization by Fu (1996) is based on the regular hexagonal crystal model, whereas Mitchell et al. (1996) use both hexagonal and random-fractal shapes.

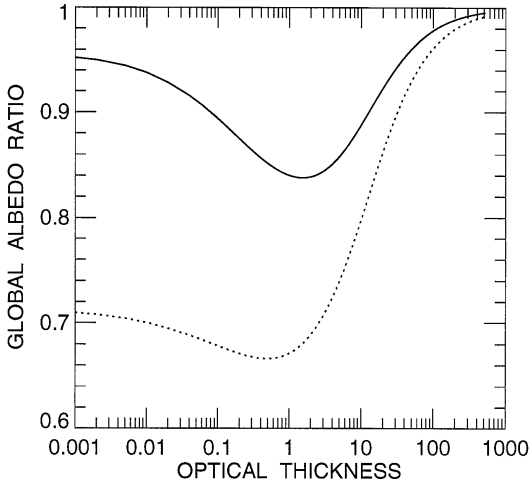

Fig. 10. Global albedo of a liquid water cloud relative to that of an optical-thickness-equivalent ice cloud composed of randomly shaped particles (dotted curve) and hexagonal columns (solid curve). The wavelength is 0.65 μm.

The fact that the Lorenz-Mie equalities $a_2(\pi) = a_1(\pi)$ and $a_4(\pi) = -a_1(\pi)$ do not, in general, hold for nonspherical particles makes measurements of the linear depolarization ratio $\delta_L = [a_1(\pi) - a_2(\pi)]/[a_1(\pi) + a_2(\pi)]$ and the circular depolarization ratio $\delta_C = [a_1(\pi) + a_4(\pi)]/[a_1(\pi) - a_4(\pi)] = 2\delta_L/(1 - \delta_L)$ the most reliable indicators of particle nonsphericity (Mishchenko and Hovenier 1995; Sassen 2000; also the chapter by Gobbi). Figure 11 shows the results of T-matrix computations of δ_L for a power law size distribution of randomly oriented nonspherical ice particles with a refractive index of 1.311 (Mishchenko and Sassen 1998). For spheroids, ε is the ratio of the largest to the smallest semi-axes. The shapes of prolate and oblate cylinders are specified by length-to-diameter and diameter-to-length ratios, respectively. The shape of second-order Chebyshev particles in a spherical coordinate system is described by the equation $R(\vartheta, \varphi) = R_0(1 + \varepsilon \cos 2\vartheta)$, where ε is a deformation parameter specifying the maximal deviation of the particle shape from that of a sphere with radius R_0 (Wiscombe and Mugnai 1988). This figure demonstrates that an interesting feature of the linear depolarization ratio for essentially all shapes considered is a rapid increase with increasing effective size parameter from 0 to about 5. This feature has been used for sizing aircraft condensation trail (contrail) particles using multi-wavelength lidar measurements (Sassen et al. 2001). Maximal δ_L values for most shapes are observed at effective size parameters close to and sometimes smaller than 10. Since geometrical optics concepts of rays, reflections, and refractions are inapplicable to wavelength and sub-wavelength sized particles, our computations suggest that multiple internal reflections in very large par-

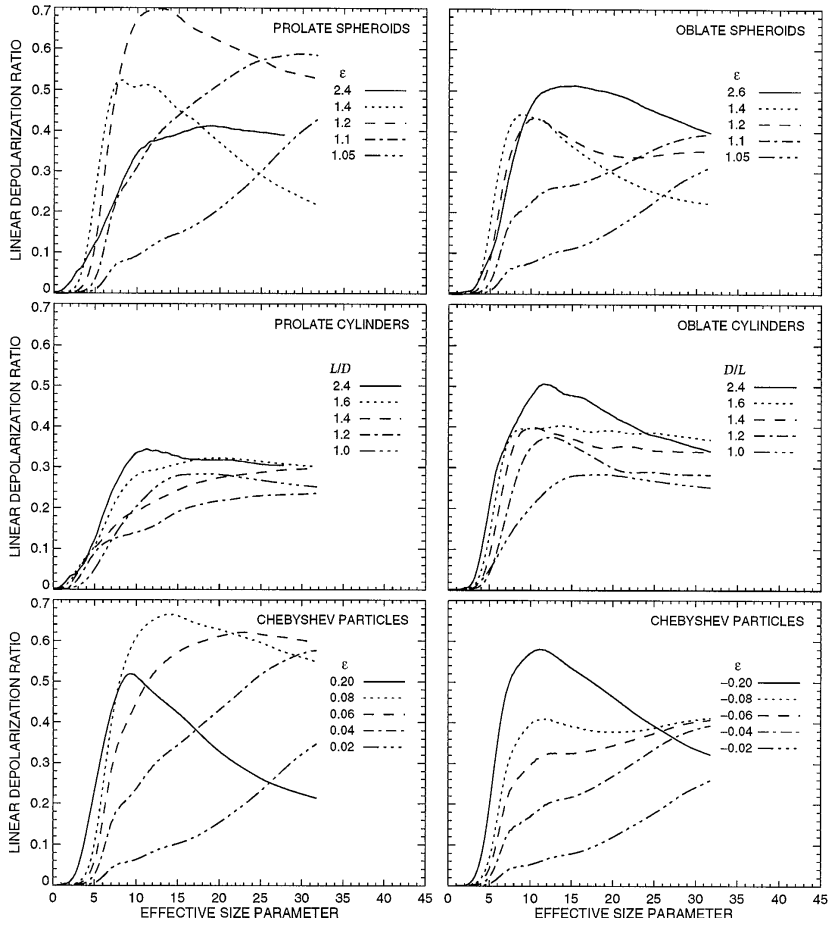

Fig. 11. Linear depolarization ratio versus effective size parameter for polydisperse, randomly oriented particles of different shapes. The refractive index is 1.311.

ticles, as discussed by Liou and Lahore (1974), are not the only mechanism of producing depolarization and not necessarily the mechanism producing maximal δ_L values. For example, the peak δ_L value for polydisperse prolate spheroids with $\varepsilon = 1.2$ is close to 0.7 and is reached at x_{eff} as small as 12.5. The computations also show that although nonzero depolarization values directly indicate the presence of nonspherical particles, there is no simple relationship between δ_L and the degree of particle asphericity (i.e., ratio of the largest to the smallest particle dimensions). Even spheroids with ε as small as 1.05 (2.5% deviation from the perfect spherical shape) and Chebyshev particles with $|\varepsilon|$ as small as 0.02 already produce strong depolarization. The largest δ_L values are produced by prolate spheroids with an aspect ratio

as small as 1.2 and Chebyshev particles with ε as small as 0.08–0.10 (8–10% deviation from a sphere). Furthermore, δ_L for spheroids and, especially, cylinders seems to saturate with increasing aspect ratio. Also of interest is that smooth scatterers (spheroids and Chebyshev particles) produce depolarization ratios comparable to and even exceeding those for sharp-edged cylinders.

The strong sensitivity of polarization and depolarization on the physical characteristics of scattering particles has been widely employed in remote sensing studies. Mishchenko and Sassen (1998) used the computations shown in Fig. 11 to explain the frequent occurrence of large δ_L values for very young contrails. Gobbi et al. (1998), Reichardt et al. (2000), and Liu and Mishchenko (2001) analyzed lidar depolarization observations of polar stratospheric clouds. Sassen (2000) and Aydin (2000) reviewed the use of lidar and radar backscattering depolarization measurements for characterizing aerosol and cloud particles and precipitation. Liou et al. (2000) discussed the potential of polarimetry in remote sensing of cirrus clouds, while Quinby-Hunt et al. (2000) described multiple applications of polarimetry in remote sensing of the marine environment.

Many other geophysical applications of electromagnetic scattering by nonspherical particles are discussed in the book edited by Mishchenko et al. (2000a), in the September/December 1999 issue of the *Journal of Quantitative Spectroscopy and Radiative Transfer*, and in the 27 December 1999 issue of the *Journal of Geophysical Research – Atmospheres*.

Acknowledgments

We thank Nadia Zakharova and Lilli Del Valle for help with graphics. This research was supported by the NASA Radiation Sciences Program managed by Donald Anderaon.

References

1. Al-Rizzo H. M. and Tranquilla J. M. (1995): Electromagnetic Wave Scattering by Highly Elongated and Geometrically Composite Objects of Large Size Parameters: The Generalized Multipole Technique. *Appl. Opt.* **34**, 3502–3521.
2. Anderson T. L., Covert D. S., Marshall S. F. et al. (1996): Performance Characteristics of a High-Sensitivity, Three-Wavelength, Total Scatter/Backscatter Nephelometer. *J. Atmos. Oceanic Technol.* **13**, 967–986.
3. Asano S. and Yamamoto G. (1975): Light Scattering by a Spheroidal Particle. *Appl. Opt.* **14**, 29–49.
4. Aydin K. (2000): Centimeter and Millimeter Wave Scattering from Nonspherical Hydrometeors. *Light Scattering by Nonspherical Particles*, eds. M. I. Mishchenko, J. W. Hovenier and L. D. Travis (Academic Press, San Diego), pp. 451–479.
5. Baran A. J., Foot J. S. and Mitchell D. L. (1998): Ice-Crystal Absorption: A Comparison Between Theory and Implications for Remote Sensing. *Appl. Opt.* **37**, 2207–2215.

6. Berenger J.-P. (1996): Three-Dimensional Perfectly Matched Layer for the Absorption of Electromagnetic Waves. *J. Comput. Phys.* **127**, 363–379.
7. Bohren C. F. and Singham S. B. (1991): Backscattering by Nonspherical Particles: A Review of Methods and Suggested New Approaches. *J. Geophys. Res.* **96**, 5269–5277.
8. Borghese F., Denti P., Toscano G. and Sindoni O. I. (1979): Electromagnetic Scattering by a Cluster of Spheres. *Appl. Opt.* **18**, 116–120.
9. Borghese F., Denti P. and Saija R. (1994): Optical Properties of Spheres Containing Several Spherical Inclusions. *Appl. Opt.* **33**, 484–493. [Errata: **34**, 5556 (1995).]
10. Bringi V. N. and Chandrasekar V. (2001): *Polarimetric Doppler Weather Radar: Principles and Applications* (Cambridge Univ. Press, Cambridge).
11. Bruning, J. H., and Lo, Y. T. (1971): Multiple Scattering of EM Waves by Spheres. *IEEE Trans. Antennas Propag.* **19**, 378–400.
12. Chandrasekhar S. (1960): *Radiative Transfer* (Dover, New York).
13. Ciric I. A. and Cooray F. R. (2000): Separation of Variables for Electromagnetic Scattering by Spheroidal Particles. *Light Scattering by Nonspherical Particles*, eds. M. I. Mishchenko, J. W. Hovenier and L. D. Travis (Academic Press, San Diego), pp. 89–130.
14. Cooray M. F. R. and Ciric I. R. (1992): Scattering of Electromagnetic Waves by a Coated Dielectric Spheroid. *J. Electromagn. Waves Applic.* **6**, 1491–1507.
15. de Haan J. F., Bosma P. B. and Hovenier J. W. (1987): The Adding Method for Multiple Scattering Calculations of Polarized Light. *Astron. Astrophys.* **183**, 371–391.
16. de Rooij W. A. and van der Stap C. C. A. H. (1984): Expansion of Mie Scattering Matrices in Generalized Spherical Functions. *Astron. Astrophys.* **131**, 237–248.
17. Deuzé J. L., Goloub P., Herman, M. et al. (2000): Estimate of the Aerosol Properties over the Ocean with POLDER. *J. Geophys. Res.* **105**, 15329–15346.
18. Doicu A., Eremin Yu. and Wriedt T. (2000): *Acoustic and Electromagnetic Scattering Analysis Using Discrete Sources* (Academic Press, San Diego).
19. Draine B. T. (2000): The Discrete Dipole Approximation for Light Scattering by Irregular Targets. *Light Scattering by Nonspherical Particles*, eds. M. I. Mishchenko, J. W. Hovenier and L. D. Travis (Academic Press, San Diego), pp. 131–145.
20. Draine B. T. and Flatau P. J. (1994): Discrete-Dipole Approximation for Scattering Calculations. *J. Opt. Soc. Am. A* **11**, 1491–1499.
21. Evans K. F. and Stephens G. L. (1995): Microwave Radiative Transfer Through Clouds Composed of Realistically Shaped Ice Crystals. Part I: Single Scattering Properties. *J. Atmos. Sci.* **52**, 2041–2057.
22. Farafonov V. G., Voshchinnikov N. V. and Somsikov V. V. (1996): Light Scattering by a Core-Mantle Spheroidal Particle. *Appl. Opt.* **35**, 5412–5426.
23. Flatau P. J. (2000): SCATTERLIB: Light Scattering Codes Library. URL: atol.ucsd.edu/∼pflatau/scatlib/.
24. Francis P. N. (1995): Some Aircraft Observations of the Scattering Properties of Ice Crystals. *J. Atmos. Sci.* **52**, 1142–1154.
25. Fu Q. (1996): An Accurate Parameterization of the Solar Radiative Properties of Cirrus Clouds for Climate Modeling. *J. Clim.* **9**, 2058–2082.

26. Fucile E., Borghese F., Denti P. and Saija R. (1993): Theoretical Description of Dynamic Light Scattering From an Assembly of Large Axially Symmetric Particles. *J. Opt. Soc. Am. A* **10**, 2611–2617.
27. Fuller K. A. (1991): Optical Resonances and Two-Sphere Systems. *Appl. Opt.* **33**, 4716–4731.
28. Fuller K. A. (1995): Scattering and Absorption Cross Sections of Compounded Spheres. III. Spheres Containing Arbitrarily Located Spherical Inhomogeneities. *J. Opt. Soc. Am. A* **12**, 893–904.
29. Fuller K. A. and Mackowski D. W. (2000): Electromagnetic Scattering by Compounded Spherical Particles. *Light Scattering by Nonspherical Particles*, eds. M. I. Mishchenko, J. W. Hovenier and L. D. Travis (Academic Press, San Diego), pp. 225–272.
30. Gayet J.-F., Auriol F., Oshchepkov S. et al. (1998): In Situ Measurements of the Scattering Phase Function of Stratocumulus, Contrails, and Cirrus. *Geophys. Res. Lett.* **25**, 971–974.
31. Gobbi G. P., Donfrancesco G. D. and Adriani A. (1998): Physical Properties of Stratospheric Clouds during the Antarctic Winter of 1995. *J. Geophys. Res.* **103**, 10859–10873.
32. Gustafson B. Å. S. (2000): Microwave Analog to Light-Scattering Measurements. *Light Scattering by Nonspherical Particles*, eds. M. I. Mishchenko, J. W. Hovenier and L. D. Travis (Academic Press, San Diego), pp. 367–390.
33. Haferman J. L. (2000): Microwave Scattering by Precipitation. *Light Scattering by Nonspherical Particles*, eds. M. I. Mishchenko, J. W. Hovenier and L. D. Travis (Academic Press, San Diego), pp. 481–524.
34. Hansen J. E. and Travis L. D. (1974): Light Scattering in Planetary Atmospheres. *Space Sci. Rev.* **16**, 527–610.
35. Havemann S. and Baran A. J. (2001): Extension of T-Matrix to Scattering of Electromagnetic Plane Waves by Non-Axisymmetric Dielectric Particles: Application to Hexagonal Ice Cylinders. *J. Quant. Spectrosc. Radiat. Transfer* **70**, 139–158.
36. Hill S. C., Hill A. C. and Barber P. W. (1984): Light Scattering by Size/Shape Distributions of Soil Particles and Spheroids. *Appl. Opt.* **23**, 1025–1031.
37. Holt A. R. (1982): The Scattering of Electromagnetic Waves by Single Hydrometeors. *Radio Sci.* **17**, 929–945.
38. Holt A. R., Uzunoglu N. K. and Evans B. G. (1978): An Integral Equation Solution to the Scattering of Electromagnetic Radiation by Dielectric Spheroids and Ellipsoids. *IEEE Trans. Antennas Propag.* **26**, 706–712.
39. Hovenier J. W. (2000): Measuring Scattering Matrices of Small Particles at Optical Wavelengths. *Light Scattering by Nonspherical Particles*, eds. M. I. Mishchenko, J. W. Hovenier and L. D. Travis (Academic Press, San Diego), pp. 355–365.
40. Hovenier J. W. and van der Mee C. V. M. (1983): Fundamental Relationships Relevant to the Transfer of Polarized Light in a Scattering Atmosphere. *Astron. Astrophys.* **128**, 1–16.
41. Hovenier J. W. and van der Mee C. V. M. (2000): Basic Relationships for Matrices Describing Scattering by Small Particles. *Light Scattering by Nonspherical Particles*, eds. M. I. Mishchenko, J. W. Hovenier and L. D. Travis (Academic Press, San Diego), pp. 61–85.
42. Hunt A. J. and Huffman D. R. (1973): A New Polarization-Modulated Light Scattering Instrument. *Rev. Sci. Instrum.* **44**, 1753–1762.

43. Jackson J. D. (1998): *Classical Electrodynamics* (Wiley, New York).
44. Jaggard D. L., Hill C., Shorthill R. W. et al. (1981): Light Scattering from Particles of Regular and Irregular Shape. *Atmos. Environ.* **15**, 2511–2519.
45. Jin J. (2002). *The Finite Element Method in Electromagnetics* (Wiley, New York).
46. Joo K. and Iskander M. F. (1990): A New Procedure of Point-Matching Method for Calculating the Absorption and Scattering of Lossy Dielectric Objects. *IEEE Trans. Antennas Propag.* **38**, 1483–1490.
47. Jones A. R. (1999): Light Scattering for Particle Characterization. *Progr. Energy Combust. Sci.* **25**, 1–53.
48. Kahn R., West R., McDonald D. et al. (1997): Sensitivity of Multiangle Remote Sensing Observations to Aerosol Sphericity. *J. Geophys. Res.* **102**, 16861–16870.
49. Kahnert F. M., Stamnes J. J. and Stamnes K. (2001): Application of the Extended Boundary Condition Method to Homogeneous Particles with Point-Group Symmetries. *Appl. Opt.* **40**, 3110–3123.
50. Khlebtsov N. G. (1992): Orientational Averaging of Light-Scattering Observables in the T-Matrix Approach. *Appl. Opt.* **31**, 5359–5365.
51. Kokhanovsky A. A. (2001): *Optics of Light Scattering Media: Problems and Solutions* (Praxis, Chichester, UK).
52. Kunz K. S. and Luebbers R. J. (1993): *Finite Difference Time Domain Method for Electromagnetics* (CRC Press, Boca Raton, FL).
53. Kurtz V. and Salib S. (1993): Scattering and Absorption of Electromagnetic Radiation by Spheroidally Shaped Particles: Computation of the Scattering Properties. *J. Imaging Sci. Technol.* **37**, 43–60.
54. Lacis A. A. and Mishchenko M. I. (1995): Climate Forcing, Climate Sensitivity, and Climate Response: A Radiative Modeling Perspective on Atmospheric Aerosols. *Aerosol Forcing of Climate*, eds. R. J. Charlson and J. Heintzenberg (Wiley, New York), pp. 11–42.
55. Laitinen H. and Lumme K. (1998): T-Matrix Method for General Star-Shaped Particles: First Results. *J. Quant. Spectrosc. Radiat. Transfer* **60**, 325–334.
56. Lakhtakia A. and Mulholland G. W. (1993): On Two Numerical Techniques for Light Scattering by Dielectric Agglomerated Structures. *J. Res. Natl. Inst. Stand. Technol.* **98**, 699–716.
57. Li L.-W., Kang X.-K. and Leong M.-S. (2002): *Spheroidal Wave Functions in Electromagnetic Theory* (Wiley, New York).
58. Liou K.-N. and Lahore H. (1974): Laser Sensing of Cloud Composition: A Backscattered Depolarization Technique. *J. Appl. Meteorol.* **13**, 257–263.
59. Liou K. N., Takano Y. and Yang P. (2000): Light Scattering and Radiative Transfer in Ice Crystal Clouds: Applications to Climate Research. *Light Scattering by Nonspherical Particles*, eds. M. I. Mishchenko, J. W. Hovenier and L. D. Travis (Academic Press, San Diego), pp. 417–449.
60. Liu L. and Mishchenko M. I. (2001): Constraints on PSC Particle Microphysics Derived from Lidar Observations. *J. Quant. Spectrosc. Radiat. Transfer* **70**, 817–831.
61. Lumme K. (2000): Scattering Properties of Interplanetary Dust Particles. *Light Scattering by Nonspherical Particles*, eds. M. I. Mishchenko, J. W. Hovenier and L. D. Travis (Academic Press, San Diego), pp. 555–583.
62. Macke A. (1993): Scattering of Light by Polyhedral Ice Crystals. *Appl. Opt.* **32**, 2780–2788.

63. Macke A., Mueller J. and Raschke E. (1996). Scattering Properties of Atmospheric Ice Crystals. *J. Atmos. Sci.* **53**, 2813–2825.
64. Mackowski D. W. (1994): Calculation of Total Cross Sections of Multiple-Sphere Clusters. *J. Opt. Soc. Am. A* **11**, 2851–2861.
65. Mackowski D. W. and Mishchenko M. I. (1996): Calculation of the T Matrix and the Scattering Matrix for Ensembles of Spheres. *J. Opt. Soc. Am. A* **13**, 2266–2278.
66. Miller E. K., Medgyesi-Mitschang L. N. and Newman E. H. (1991): *Computational Electromagnetics: Frequency Domain Method of Moments* (IEEE Press, New York).
67. Mishchenko M. I. (1991): Light Scattering by Randomly Oriented Axially Symmetric Particles. *J. Opt. Soc. Am. A* **8**, 871–882. [Errata: **9**, 497 (1992).]
68. Mishchenko M. I. and Hovenier J. W. (1995): Depolarization of Light Backscattered by Randomly Oriented Nonspherical Particles. *Opt. Lett.* **20**, 1356–1358.
69. Mishchenko M. I. and Macke A. (1998): Incorporation of Physical Optics Effects and Computation of the Legendre Expansion for Ray-Tracing Phase Functions Involving δ-Function Transmission. *J. Geophys. Res.* **103**, 1799–1805.
70. Mishchenko M. I. and Macke A. (1999): How Big Should Hexagonal Ice Crystals Be to Produce Halos? *Appl. Opt.* **38**, 1626–1629.
71. Mishchenko M. I. and Sassen K. (1998): Depolarization of Lidar Returns by Small Ice Crystals: An Application to Contrails. *Geophys. Res. Lett.* **25**, 309–312.
72. Mishchenko M. I. and Travis L. D. (1998): Capabilities and Limitations of a Current FORTRAN Implementation of the T-Matrix Method for Randomly Oriented, Rotationally Symmetric Scatterers. *J. Quant. Spectrosc. Radiat. Transfer* **60**, 309–324.
73. Mishchenko M. I., Mackowski D. W. and Travis L. D. (1995): Scattering of Light by Bispheres with Touching and Separated Components. *Appl. Opt.* **34**, 4589–4599.
74. Mishchenko M. I., Travis L. D. and Macke A. (1996a): Scattering of Light by Polydisperse, Randomly Oriented, Finite Circular Cylinders. *Appl. Opt.* **35**, 4927–4940.
75. Mishchenko M. I., Travis L. D. and Mackowski D. W. (1996b): T-Matrix Computations of Light Scattering by Nonspherical Particles: A Review. *J. Quant. Spectrosc. Radiat. Transfer* **55**, 535–575.
76. Mishchenko M. I., Rossow W. B., Make A. and Lacis A. A. (1996c): Sensitivity of Cirrus Cloud Albedo, Bidirectional Reflectance and Optical Thickness Retrieval Accuracy to Ice Particle Shape. *J. Geophys. Res.* **101**, 16973–16985.
77. Mishchenko M. I., Travis L. D., Kahn R. A. and West R. A. (1997): Modeling Phase Functions for Dustlike Tropospheric Aerosols Using a Shape Mixture of Randomly Oriented Polydisperse Spheroids. *J. Geophys. Res.* **102**, 16831–16847.
78. Mishchenko M. I., Hovenier J. W. and Travis L. D., eds. (2000a): *Light Scattering by Nonspherical Particles* (Academic Press, San Diego).
79. Mishchenko M. I., Hovenier J. W. and Travis L. D. (2000b): Concepts, Terms, Notation. *Light Scattering by Nonspherical Particles*, eds. M. I. Mishchenko, J. W. Hovenier and L. D. Travis (Academic Press, San Diego), pp. 3–27.

80. Mishchenko M. I., Travis L. D. and Lacis A. A. (2002): *Scattering, Absorption, and Emission of Light by Small Particles* (Cambridge Univ. Press, Cambridge).
81. Mitchell D. L., Macke A. and Liu Y. (1996): Modeling Cirrus Clouds. II: Treatment of Radiative Properties. *J. Atmos. Sci.* **53**, 2967–2988.
82. Morgan M. A. (1980): Finite Element Computation of Microwave Scattering by Raindrops. *Radio Sci.* **15**, 1109–1119.
83. Morrison J. A. and Cross M.-J. (1974): Scattering of a Plane Electromagnetic Wave by Axisymmetric Raindrops. *Bell Syst. Tech. J.* **53**, 955–1019.
84. Muinonen K. (1989): Scattering of Light by Crystals: A Modified Kirchhoff Approximation. *Appl. Opt.* **28**, 3044–3050.
85. Muinonen K. (2000): Light Scattering by Stochastically Shaped Particles. *Light Scattering by Nonspherical Particles*, eds. M. I. Mishchenko, J. W. Hovenier and L. D. Travis (Academic Press, San Diego), pp. 323–352.
86. Oguchi T. (1973): Scattering Properties of Oblate Raindrops and Cross Polarization of Radio Waves Due to Rain: Calculations at 19.3 and 34.8 GHz. *J. Radio Res. Lab. Japan* **20**, 79–118.
87. Okamoto H., Macke A., Quante M. and Raschke E. (1995): Modeling of Backscattering by Nonspherical Ice Particles for the Interpretation of Cloud Radar Signals at 94 Ghz. An Error Analysis. *Beitr. Phys. Atmos.* **68**, 319–334.
88. Onaka T. (1980): Light Scattering by Spheroidal Grains. *Ann. Tokyo Astron. Observ.* **18**, 1–54.
89. Peltoniemi J. I., Lumme K., Muinonen K. and Irvine W. M. (1989): Scattering of Light by Stochastically Rough Particles. *Appl. Opt.* **28**, 4088–4095.
90. Perry R. J., Hunt A. J. and Huffman D. R. (1978): Experimental Determination of Mueller Scattering Matrices for Nonspherical Particles. *Appl. Opt.* **17**, 2700–2710.
91. Peterson B. and Ström S. (1973): T Matrix for Electromagnetic Scattering from an Arbitrary Number of Scatterers and Representations of E(3)*. *Phys. Rev. D* **8**, 3661–3678.
92. Peterson B. and Ström S. (1974): T-Matrix Formulation of Electromagnetic Scattering From Multilayered Scatterers. *Phys. Rev. D* **10**, 2670–2684.
93. Peterson A. F., Ray S. L. and Mittra R. (1998): *Computational Methods for Electromagnetics* (IEEE Press, New York).
94. Purcell E. M. and Pennypacker C. R. (1973): Scattering and Absorption of Light by Nonspherical Dielectric Grains. *Astrophys. J.* **186**, 705–714.
95. Quinby-Hunt M. S., Hull P. G. and Hunt A. J. (2000): Polarized Light Scattering in the Marine Environment. *Light Scattering by Nonspherical Particles*, eds. M. I. Mishchenko, J. W. Hovenier and L. D. Travis (Academic Press, San Diego), pp. 525–554.
96. Ravey J.-C. and Mazeron P. (1982): Light Scattering in the Physical Optics Approximation: Application to Large Spheroids. *J. Opt. (Paris)* **13**, 273–282.
97. Rayleigh, Lord (1897): On the Incidence of Aerial and Electric Waves Upon Small Obstacles in the Form of Ellipsoids or Elliptic Cylinders, and on the Passage of Electric Waves through a Circular Aperture in a Conducting Screen. *Phil. Mag.* **44**, 28–52.
98. Reagan J. A., McCormick M. P. and Spinhirne J. D. (1989): Lidar Sensing of Aerosols and Clouds in the Troposphere and Stratosphere. *Proc. IEEE* **77**, 433–448.

99. Reichardt J., Tsias A. and Behrendt A. (2000): Optical Properties of PSC Ia–Enhanced at UV and Visible Wavelengths: Model and Observations. *Geophys. Res. Lett.* **27**, 201–204.
100. Rossow W. B. and Schiffer R. A. (1999): Advances in Understanding Clouds from ISCCP. *Bull. Am. Meteorol. Soc.* **80**, 2261–2287.
101. Sassen K. (2000): Lidar Backscatter Depolarization Technique for Cloud and Aerosol Research. *Light Scattering by Nonspherical Particles*, eds. M. I. Mishchenko, J. W. Hovenier and L. D. Travis (Academic Press, San Diego), pp. 393–416.
102. Sassen, K., Comstock, J. M., Wang, Zh., and Mace, G. G. (2001). Cloud and aerosol research capabilities at FARS: The Facility for Atmospheric Remote Sensing. *Bull. Am. Meteorol. Soc.* **82**, 1119–1138.
103. Saxon D. S. (1955a): Tensor Scattering Matrix for the Electromagnetic Field. *Phys. Rev.* **100**, 1771–1775.
104. Saxon D. S. (1955b): Lectures on the Scattering of Light (Scientific Report No. 9, Department of Meteorology, University of California at Los Angeles).
105. Silvester P. P. and Ferrari R. L. (1996): *Finite Elements for Electrical Engineers* (Cambridge Univ. Press, New York).
106. Stephens G. L. (1994): *Remote Sensing of the Lower Atmosphere* (Oxford Univ. Press, New York).
107. Sun W. and Fu Q. (2000): Finite-Difference Time-Domain Solution of Light Scattering by Dielectric Particles with Large Complex Refractive Indices. *Appl. Opt.* **39**, 5569–5578.
108. Taflove A. and Hagness S. C. (2000): *Computational Electrodynamics: The Finite-Difference Time-Domain Method* (Artech House, Boston).
109. Takano Y. and Liou K. N. (1995): Solar Radiative Transfer in Cirrus Clouds. III: Light Scattering by Irregular Ice Crystals. *J. Atmos. Sci.* **52**, 818–837.
110. Tsang L., Kong J. A. and Shin R. T. (1985): *Theory of Microwave Remote Sensing* (Wiley, New York).
111. van de Hulst H. C. (1957): *Light Scattering by Small Particles* (Wiley, New York).
112. van der Mee C. V. M. and Hovenier J. W. (1990): Expansion Coefficients in Polarized Light Transfer. *Astron. Astrophys.* **228**, 559–568.
113. Videen G., Ngo D., Chýlek P. and Pinnick R. G. (1995): Light Scattering from a Sphere with an Irregular Inclusion. *J. Opt. Soc. Am. A* **12**, 922–928.
114. Volakis J. L., Chatterjee A. and Kempel L. C. (1998): *Finite Element Method for Electromagnetics* (IEEE Press, New York).
115. Volten H., Muñoz O., Rol E. et al. (2001): Scattering Matrices of Mineral Aerosol Particles at 441.6 and 632.8 nm. *J. Geophys. Res.* **106**, 17375–17402.
116. Voshchinnikov N. V. and Farafonov V. G. (1993): Optical Properties of Spheroidal Particles. *Astrophys. Space Sci.* **204**, 19–86.
117. Waterman P. C. (1971): Symmetry, Unitarity, and Geometry in Electromagnetic Scattering. *Phys. Rev. D.* **3**, 825–839.
118. West R. A. (1991): Optical Properties of Aggregate Particles Whose Outer Diameter is Comparable to the Wavelength. *Appl. Opt.* **30**, 5316–5324.
119. Wielaard D. J., Mishchenko M. I., Macke A. and Carlson B. E. (1997): Improved **T**-Matrix Computations for Large, Nonabsorbing and Weakly Absorbing Nonspherical Particles and Comparison with Geometrical-Optics Approximation. *Appl. Opt.* **36**, 4305–4313.

120. Wiscombe W. J. and Mugnai A. (1988): Scattering from Nonspherical Chebyshev Particles. 2: Means of Angular Scattering Patterns. *Appl. Opt.* **27**, 2405–2421.
121. Wriedt T., ed. (1999): *Generalized Multipole Techniques for Electromagnetic and Light Scattering* (Elsevier, Amsterdam).
122. Wriedt T. (2000): Electromagnetic Scattering Programs. URL: www.t-matrix.de.
123. Yang P. and Liou K. N. (1996): Finite-Difference Time Domain Method for Light Scattering by Small Ice Crystals in Three-Dimensional Space. *J. Opt. Soc. Am. A* **13**, 2072–2085.
124. Yang P. and Liou K. N. (2000): Finite Difference Time Domain Method for Light Scattering by Nonspherical and Inhomogeneous Particles. *Light Scattering by Nonspherical Particles*, eds. M. I. Mishchenko, J. W. Hovenier and L. D. Travis (Academic Press, San Diego), pp. 173–221.
125. Yee K. S. (1966): Numerical Solution of Initial Boundary Value Problems Involving Maxwell's Equations in Isotropic Media. *IEEE Trans. Antennas Propag.* **14**, 302–307.
126. Zakharova N. T. and Mishchenko M. I. (2000): Scattering Properties of Needlelike and Platelike Ice Spheroids with Moderate Size Parameters. *Appl. Opt.* **39**, 5052–5057.
127. Zakharova N. T. and Mishchenko M. I. (2001): Scattering by Randomly Oriented Thin Ice Disks with Moderate Equivalent-Sphere Size Parameters. *J. Quant. Spectrosc. Radiat. Transfer* **70**, 465–471.